OXFORD

Cerebral Cortex, March 2021;31: 1744–1762

doi: 10.1093/cercor/bhaa323
Advance Access Publication Date: 24 November 2020
Original Article

ORIGINAL ARTICLE

Temporally Distinct Roles for the Zinc Finger Transcription Factor Sp8 in the Generation and Migration of Dorsal Lateral Ganglionic Eminence (dLGE)-Derived Neuronal Subtypes in the Mouse

J. Kuerbitz[1,4], M. Madhavan[1], L.A. Ehrman[1,3], V. Kohli[3], R.R. Waclaw[1,3] and K. Campbell[1,2]

[1]Divisions of Developmental Biology, Cincinnati Children's Hospital Medical Center, Cincinnati, OH 45229, USA, [2]Divisions of Neurosurgery, Cincinnati Children's Hospital Medical Center, University of Cincinnati College of Medicine, Cincinnati, OH 45229, USA, [3]Divisions of Experimental Hematology and Cancer Biology, Cincinnati Children's Hospital Medical Center, University of Cincinnati College of Medicine, Cincinnati, OH 45229, USA and [4]Medical-Scientist Training Program, University of Cincinnati College of Medicine, Cincinnati, OH 45229, USA

Address correspondence to Kenneth Campbell. Email: kenneth.campbell@cchmc.org.

Abstract

Progenitors in the dorsal lateral ganglionic eminence (dLGE) are known to give rise to olfactory bulb (OB) interneurons and intercalated cells (ITCs) of the amygdala. The dLGE enriched transcription factor Sp8 is required for the normal generation of ITCs as well as OB interneurons, particularly the calretinin (CR)-expressing subtype. In this study, we used a genetic gain-of-function approach in mice to examine the roles Sp8 plays in controlling the development of dLGE-derived neuronal subtypes. Misexpression of *Sp8* throughout the ventral telencephalic subventricular zone (SVZ) from early embryonic stages, led to an increased generation of ITCs which was dependent on *Tshz1* gene dosage. Additionally, *Sp8* misexpression impaired rostral migration of OB interneurons with clusters of CR interneurons seen in the SVZ along with decreased differentiation of calbindin OB interneurons. *Sp8* misexpression throughout the ventral telencephalon also reduced ventral LGE neuronal subtypes including striatal projection neurons. Delaying *Sp8* misexpression until E14–15 rescued the striatal and amygdala phenotypes but only partially rescued OB interneuron reductions, consistent with an early window of striatal and amygdala neurogenesis and ongoing OB interneuron generation at this late stage. Our results demonstrate critical roles for the timing and neuronal cell-type specificity of Sp8 expression in mouse LGE neurogenesis.

Key words: intercalated cells (ITCs), mouse, neurogenesis, olfactory bulb (OB), striatum

Introduction

Amygdala circuitry has been implicated in the pathology of many neuropsychiatric illnesses including depression and anxiety disorders (Maletic et al. 2007; Walker 2007; Duval et al. 2015). Neurons comprising these amygdala circuits are derived from a subpallial progenitor zone called the lateral ganglionic eminence (LGE) as well as the ventral pallium (VP) and lateral pallium (LP) (Cocas et al. 2009; Hirata et al. 2009; Waclaw et al. 2010). The LGE can be further subdivided into 2 compartments. The dorsal LGE (dLGE) gives rise to a population of inhibitory neurons in the amygdala known as intercalated cells (ITCs) (Waclaw et al. 2010; Kuerbitz et al. 2018) as well as the bulk of olfactory bulb (OB) interneurons (Stenman et al. 2003a; Lledo et al. 2008). In contrast, progenitors in the ventral LGE (vLGE)

predominantly give rise to GABAergic medium spiny neurons that constitute the major neuronal subtype within the striatum (Stenman et al. 2003a; Waclaw et al. 2009) as well as the central amygdala (CeA) (Waclaw et al. 2010). The dLGE and vLGE exhibit distinct molecular profiles. The dLGE is characterized by high levels of the transcription factors *Gsx2*, *Er81*, *Sp8*, and *Tshz1*, whereas the vLGE is distinguished by expression of *Isl1*, *Nolz1*, *Sox8*, and *Ebf1* (Toresson et al. 2000; Yun et al. 2001; Stenman et al. 2003a; Chang et al. 2004; Caubit et al. 2005; Waclaw et al. 2006, 2009; Merchan-Sala et al. 2017; Kuerbitz et al. 2018).

Progenitors within the dLGE and vLGE give rise to anatomically and molecularly heterogeneous populations of neurons. vLGE derived striatal projection neurons (SPNs) comprise dopamine D1 receptor (Drd1) expressing direct pathway (d)SPNs which project to the substantia nigra and dopamine D2 receptor (Drd2) expressing indirect pathway (i)SPNs which project to the globus pallidus (Gerfen et al. 1990; Stenman et al. 2003a). By contrast, the dLGE produces ITCs that migrate laterally into the amygdala region and OB interneurons that migrate rostrally to populate either the granule cell layer (GCL) or glomerular layer (GL) of the OB. Most GCL neurons express *Meis2* and *Mef2c* and can be classified according to their expression of calretinin (CR) or 5 T4 (López-Juárez et al. 2013; Batista-Brito et al. 2014; Qin et al. 2016). GL neurons broadly express *Meis2* and can be defined by the exclusive expression of either tyrosine hydroxylase (TH), calbindin (CB) or CR (Kosaka et al. 1985, 1998; Allen et al. 2007; Parrish-Aungst et al. 2007; Nagayama et al. 2014). In contrast to the anterior migration of OB interneurons in the RMS, ITCs migrate ventrolaterally from the dLGE via the lateral migratory stream (LMS) (Bayer et al. 1991; Carney et al. 2006; Cocas et al. 2011) and are marked by expression of *Foxp2*, *Meis2*, *Drd1*, and μ-opioid receptor (μOR) (Fremeau et al. 1991; Stenman et al. 2003b; Jacobsen et al. 2006; Kaoru et al. 2010; Waclaw et al. 2010). The means by which neural precursors originating from common germinal zones give rise to anatomically and molecularly distinct populations of mature neurons is only beginning to be understood (Mayer et al. 2018).

The zinc finger transcription factor Sp8 is expressed in the dLGE subventricular zone (SVZ) and at postnatal timepoints, in neuroblasts migrating to the OB via the rostral migratory stream (RMS) (Waclaw et al. 2006; López-Juárez et al. 2013; Fujiwara and Cave 2016). Sp8 remains expressed in CR-expressing interneurons in the OB, while limited expression has also been observed in either the TH or CB-expressing GL populations (Waclaw et al. 2006; Allen et al. 2007; Kosaka and Kosaka 2012; Fujiwara and Cave 2016). Conditional *Sp8* mutant mice show impaired generation of CR^+ interneurons in the GL (Waclaw et al. 2006) and parvalbumin$^+$ (PV^+) interneurons in the external plexiform layer (EPL) of the mutant OB (Li et al. 2011). Additionally, these mutants exhibit reduced numbers of ITCs (Waclaw et al. 2010). *Sp8/Sp9* double mutants have been reported to display severely reduced numbers of GABAergic and dopaminergic GL interneurons as well as impaired radial migration among SVZ derived OB neuroblasts (Li et al. 2018). Despite the clear requirements for this transcription factor in many dLGE-derived neuronal subtypes, its specific temporal roles in the generation of these diverse neuronal subtypes remain only partially defined.

In this study, we have utilized a misexpression system employing a *Dlx5/6-tTA* transgene to drive Sp8 misexpression throughout the developing ventral telencephalic SVZ. Misexpression of *Sp8* throughout the LGE SVZ resulted in a significant increase in ITCs at postnatal stages which was dependent on *Tshz1* gene dosage. Within the OB, Foxp2-expressing CB interneurons and dopaminergic interneurons were significantly reduced, and while no significant changes were observed in OB CR interneurons, a significant increase in CR interneurons was observed in clumps along the lateral ventricular wall. Additionally, *Sp8* misexpression severely reduced vLGE neuronal fates (i.e., SPNs). To determine whether Sp8 regulates distinct neuronal fates at different embryonic timepoints, we utilized a doxycycline (Dox)-based approach to delay *Sp8* misexpression in the LGE SVZ until after E15. In the delayed misexpression animals, the ITC and SPN phenotypes appear normalized whereas the OB phenotype is only partially improved. These findings indicate that *Sp8*'s role in the generation of ITCs is limited to early stages of embryonic neurogenesis, whereas it continues to influence OB neurogenesis at late embryonic and postnatal timepoints.

Materials and Methods

Animals

Animal protocols were implemented according to the Cincinnati Children's Hospital Medical Center (CCHMC) Institutional Animal Care and Use Committee and the National Institutes of Health guidelines. Mice used in the present study were maintained on an outbred (CD1) background.

TetO-Sp8-IRES-EGFP(IE) mice were generated and characterized as described previously (Borello et al. 2014). *TetO-Sp8-IE* animals were genotyped with the primer pairs Sp8-CD-Sense (5′-CGTTCGTGTGCAATTGGCTG-3′) and IRES-Anti (5′-AAACGCACACCGGCCTTATT-3′). To generate *TetO-IRES-EGFP (TetO-IE)* mice, we released the 2.4-kb $TetO_7$-polylinker-IRES-EGFP fragment from the pTetO_7-polylinker-IRES-EGFP vector (Waclaw et al. 2009) using *Ahd1* and *Asc1* followed by gel purification of the released product. Pronuclear injections of this fragment were performed by the transgenic core at CCHMC. *TetO-IE* mice were genotyped with the primer pair GFP57–5′ (5′-AGCAAAGACCCCAACGAGAAGC-3′) and GFP57–3′ (5′-CCAACAACAGATGGCTGGCAAC-3′) or EGFP65–5′ (5′-GACGTAAACGGCCACAAGTTC-3′), and EGFP65–3′ (5′-CTTCAGCT CGATGCGGTTCA-3′).

To generate *Dlx5/6-tTA* animals, the tetracycline transactivator construct (tTA) with a modified Kozak sequence (a gift from Dr Jeffrey Robbins, Cincinnati Children's Hospital Medical Center, Cincinnati, OH) was subcloned into the PIRES vector (Clontech, Palo Alto, CA) upstream of the Sv40 polyadenylation sequence. The tTA-Sv40 construct was then subcloned into a P19 vector containing the mouse id6/id5 (i.e., *Dlx5/6*) enhancer (Zerucha et al. 2000). Pronuclear injections of the resulting construct were performed by the transgenic core at CCHMC. *Dlx5/6-tTA* animals were genotyped with the primers rtTA-5′ (5′-AGCGCATTAGAGCTGCTTAATGAGGTC-3′) and rtTA-3′ (5′-GTCGTAATAATGGCGGCATACTATC-3′).

Sp8-EGFP BAC (RRID:MMRRC_034608-UCD) mice were obtained from GENSAT (Gong et al. 2003). *Sp8-GFP* mice were genotyped with the primer pair GFP57–5′ (5′-AGCAAAGACCCCAA CGAGAAGC-3′) and GFP57–3′ (5′-CCAACAACAGATGGCTGGCAAC-3′) or EGFP65–5′ (5′-GACGTAAACGGCCACAAGTTC-3′) and EGFP65–3′ (5′-CTTCAGCTCGATGCGGTTCA-3′). *Tshz1*$^{RA/+}$ mice were generated and genotyped as described previously (Ragancokova et al. 2014; Kuerbitz et al. 2018). *Isl1*^{creER} mice (RRID:IMSR_JAX:029566) were obtained from the Jackson Laboratory and were genotyped with the primer pair Cre66–5′ (5′-TTGGCAGAACGAAA ACGCTG-3′) and Cre66–3′ (5′-ACCATTGCCCCTGTTTCA

CT-3′). *Rosa*^{tdTomato} mice (RRID:IMSR_JAX:007914) were obtained from the Jackson Laboratory and were genotyped with the primer pair Rosa-tdTomato-5′ (5′-GGCATTAAAGCAGCGTATCC-3′) and Rosa-tdTomato-3′ (5′-CTGTTCCTGTACGGCATGG-3′). *Rosa*^{rTA} mice (RRID:IMSR_JAX:011008) were obtained from the Jackson Laboratory and were genotyped with the primer pair rtTA-5′ (5-AGCGCATTAGAGCTGCTTAATGAGGTC-3′) and rtTA-3 (5′-GTCGTAATAATGGCGGCATACTATC-3′).

To stage embryos, the day of vaginal plug detection was considered embryonic day 0.5 (E0.5). Doxycycline hyclate (Dox, Sigma) was administered at a concentration of 0.02 mg/mL via drinking water to pregnant females to suppress transgene activation as described previously (Waclaw et al. 2009; Chapman et al. 2013; Borello et al. 2014).

Tamoxifen was dissolved in corn oil at 10 mg/mL and administered to pregnant *Isl1*^{creER} dams at E11.5 (75 mg/kg i.p.) and at E13.5 (50 mg/kg i.p.). Pregnant dams were euthanized on E17.5 and pups were collected and genotyped.

Following euthanasia with CO_2, E13.5 embryonic heads were fixed intact in 4% paraformaldehyde (PFA) overnight whereas for all other timepoints (e.g., E15.5 onward to postnatal stages), brains were dissected prior to overnight fixation in 4% PFA. After overnight fixation, brains were washed in PBS for 2 h and cryoprotected in sucrose solution for 48 h. Embryonic and P3 brains were cryoprotected in 30% sucrose, frozen in NEG-50 (Richard-Allan Scientific, Kalamazoo, MI) and stored at −80°C until sectioning. Embryonic and P3 brains were sectioned into 12 µm sections on a cryostat. P21 brains were cryoprotected in 13% sucrose, flash frozen, and stored at −80°C until sectioning. P21 brains were sectioned into 35 µm floating sections on a sliding microtome and placed in PBS. For long-term storage, floating sections were transferred to a solution of 30% glycerol/30% ethylene glycol in PBS and stored at −20°C.

Immunohistology

P21 sections were stained free-floating prior to mounting on slides. P3 and embryonic sections were mounted on slides immediately after cryosectioning and subsequently stained. Immunohistochemical staining was carried out using the method described in Olsson et al. 1997. Immunofluorescence staining was carried out as described in Qin et al. 2016. The following primary antibodies were used at the indicated concentrations: guinea pig anti-µOR (1:1000, Millipore, RRID:AB_117511); goat anti-calretinin (CR, 1:2000, Millipore, RRID: AB_90764); rabbit anti-calbindin D-28 k (CB, 1:4000, Swant, RRID:AB_2314070); guinea pig anti-DARPP-32 (1:500, Chemicon, RRID:AB_2252837); guinea pig anti-Doublecortin (1:3000, Millipore, RRID:AB_1586992); rabbit anti-DsRed (1:1000, Living Colors, AB_10013483); rabbit anti-Foxp1 (1:5000, Abcam, RRID:AB_2341188); goat anti-Foxp2 (1:1000, Abcam RRID:AB_1268914); chicken anti-GFP (1:1000, Aves Labs, RRID:AB_10000240); goat anti-GFP (1:1000, Abcam, RRID:AB_305635); rabbit anti-GFP (1:500, Invitrogen, RRID:AB_221477); rabbit anti-Gsx2 (1:5000, Toresson et al. 2000); rabbit anti-Meis2 (1:500, Atlas Antibodies, RRID:AB_611953); rabbit anti-parvalbumin (1:1000, Swant, RRID:AB_10000344); rabbit anti-Pax6 (1:1000, Biolegend, RRID:AB_291612); goat anti-Sp8 (1:5000, Santa Cruz, RRID:AB_2194626); chicken anti-tyrosine hydroxylase (TH, 1:1000, AVES, RRID:AB_10013440). Primary antibody staining was followed by staining with the following secondary antibodies at the indicated concentrations: donkey anti-chicken conjugated with Alexa 488 or Alexa 647 (1:400, Jackson Immunoresearch, RRID:AB_2340375 and AB_2340380, respectively); donkey anti-goat conjugated with Alexa 594 or Alexa 647 (1:400, Jackson Immunoresearch, RRID:AB_2340434 and AB_2340438, respectively); donkey anti-guinea pig conjugated with Alexa 594 (1:400 Jackson Immunoresearch, RRID:AB_2340475); and donkey anti-rabbit conjugated with Alexa 488, Alexa 594, or Alexa 647 (1:400 Jackson Immunoresearch, RRID: AB_2340619, AB_2340622, and AB_2340625, respectively). For immunohistochemical staining, donkey anti-guinea pig secondary antibody conjugated with biotin (1:200, Vector Laboratories, RRID:AB_2336132) was used. Secondary antibody treatment was followed by treatment with the ABC horseradish peroxidase kit (both reagents 1:200, Vectastain, RRID:AB_2336827) according to manufacturer instructions.

Following immunohistochemical staining, digital micrographs were acquired using a Nikon Ni-E upright widefield microscope. Following immunofluorescent staining, digital micrographs were acquired using either a Nikon A1 LUN-A or a Nikon A1R LUN-V laser scanning inverted confocal microscope. Images were pseudocolored and converted to TIFFs using Nikon NIS-elements software. Color levels were subsequently adjusted using Adobe Photoshop CS6 software, with equal adjustments being applied to control and experimental images.

In Situ Hybridization

In situ hybridization was carried out on cryosections as described by Toresson et al. (1999). Antisense probe to the *Tshz1* coding domain was generated using the primer pair Tshz15: (5′-GCATCAAGAAGCAACCGGAC-3′) and T3-Tshz13: (5′-AATTAACCCTCACTAAAGGGAGACTTGGGAGTCAGACGACCTG-3′). Hybridization was performed overnight at 65°C. Following development, digital micrographs were acquired using a Nikon Ni-E upright widefield microscope. Images were white-balanced and converted to TIFFs using Nikon NIS-elements software.

Experimental Design and Statistical Analysis

For cell counts, 2–4 sections from 3 to 6 mice/embryos per condition were quantified for each analysis. Ages, regions, and *n*-values are reported in the text and figures. For all cell counts except for TH, all cells labeled by each marker in the region of interest were counted using Nikon NIS-elements software. The morphology of TH$^+$ cells made automated quantification difficult, so TH$^+$ cells were counted manually by researchers blind to genotype. For cell number counts, the average number of cells per section are reported. For cell density counts, total cell number was normalized to the total area quantified for each animal. For in situ hybridization and immunohistochemistry quantification, intensity thresholds were defined based on background levels across the dataset, and the area exceeding this threshold in each image was quantified using Nikon NIS-elements software. *P*-values for experiments comparing *Sp8* misexpressing animals to controls were calculated using a two-tailed *t*-test using R. The variance parameter was determined based on the result of an *F* test. *P*-values comparing marker coexpression between different cell populations (Fig. 1) were calculated using a one-way ANOVA followed by post hoc Tukey HSD tests for between-group comparisons in R. *P*-values comparing cell counts or in situ quantifications across 2 distinct experimental factors (Figs 4 and 9) were calculated using a two-way ANOVA followed by post hoc Tukey HSD tests for between-group comparisons in R. Correlations are reported as Pearson's

product moment coefficients with *P*-values calculated assuming $n-2$ degrees of freedom. Bar graphs depict mean ± SEM. All fold changes reported represent (experimental value−control value)/control value. Significance was set at $P \leq 0.05$.

Results

Sp8 Expressing Progenitors Differentially Give Rise to OB Interneuron Subpopulations

In agreement with previous studies, immunostaining for Sp8 in the embryonic mouse brain revealed robust expression in the SVZ of the dLGE (Fig. 1A) as well as in the forming GL and GCL of the embryonic OB (Fig. 1B) (Waclaw et al. 2006, 2009; Sahara et al. 2007; Borello et al. 2014). At caudal levels, a narrow stream could be detected between the dLGE and the developing amygdala (Fig. 1C), as previously described (Waclaw et al. 2006). Previous research has established the postnatal SVZ of the rodent as a continuous site of OB neurogenesis throughout adulthood (Lois and Alvarez-Buylla 1994). At adult timepoints, Sp8 expression was detected in the mouse SVZ (Fig. 1D), the GCL and GL of the OB (Fig. 1E), and in the RMS (Fig. 1F), in line with previous reports (Wei et al. 2011; Chen et al. 2012; Wang et al. 2014). To identify cells derived from *Sp8* expressing progenitors, we utilized a *Sp8-EGFP* BAC transgenic mouse line from GENSAT, taking advantage of the stability of GFP protein as a short-term fate-mapping tool (Gong et al. 2003). EGFP-expressing cells could be detected in *Sp8* expressing domains including the embryonic dLGE (Fig. 1G) and early postnatal OB (Fig. 1H) as well as in the early postnatal ITCs in the amygdala (Fig. 1I), a population previously reported to be derived from Sp8 expressing dLGE progenitors (Waclaw et al. 2010; Kuerbitz et al. 2018). Interestingly, cells expressing moderate levels of EGFP were also detected in vLGE derivatives such as the striatum, which probably reflects a refinement to the high-expressing *Sp8* domains over development. At P10, EGFP expression was observed in many cells in the GL, the majority (i.e., 68.3%) of which were Sp8 expressing cells (Fig. 1J,Q). The fact that approximately 30% of EGFP$^+$ GL cells were not Sp8$^+$ suggests that a considerable portion of Sp8$^+$ neuroblasts may downregulate this factor as they mature into GL neurons, in line with previous reports (Gaborieau et al. 2018). Previous research has shown Sp8 coexpression in the OB with the calcium binding protein CR (Waclaw et al. 2006; Allen et al. 2007; Kosaka and Kosaka 2012; Fujiwara and Cave 2016). Indeed, Sp8 is required for the normal generation of the CR$^+$ subpopulation of OB interneurons (Waclaw et al. 2006). Colabeling of juvenile *Sp8-EGFP* brains the with the OB interneuron markers CB, TH, and CR revealed that EGFP-expressing cells were primarily of the CR$^+$ interneuron subtype as compared to the CB$^+$ or TH$^+$ subpopulations (Fig 1, K–M). A one-way ANOVA ($F_{(2,8)} = 110.8$, $P = 1.47 \times 10^{-6}$) revealed that EGFP positive cells were significantly more likely to coexpress CR (19.9%; $n = 3$) than they were CB (5.0%; $n = 4$, $p = 2.3 \times 10^{-6}$,) or TH (5.8%; $n = 4$, $P = 3.4 \times 10^{-6}$) (Fig. 1Q). We previously found that CR$^+$ GL neurons comprise almost 50% of all Sp8$^+$ GL cells (Waclaw et al. 2006) thus it may be that the short-term fate map using the *Sp8-EGFP* BAC mice may overreport for Sp8-derived GL neurons. Nevertheless, this genetic tool affirms that Sp8-expressing neuroblasts preferentially give rise to CR$^+$ GL neurons as compared to the CB and TH subtypes. CB$^+$ neurons have previously been reported to coexpress Foxp2 (Fujiwara and Cave 2016). Likewise, previous research has reported that TH$^+$ (i.e., dopaminergic) GL cells coexpress Pax6 and that it is essential for TH$^+$ interneuron

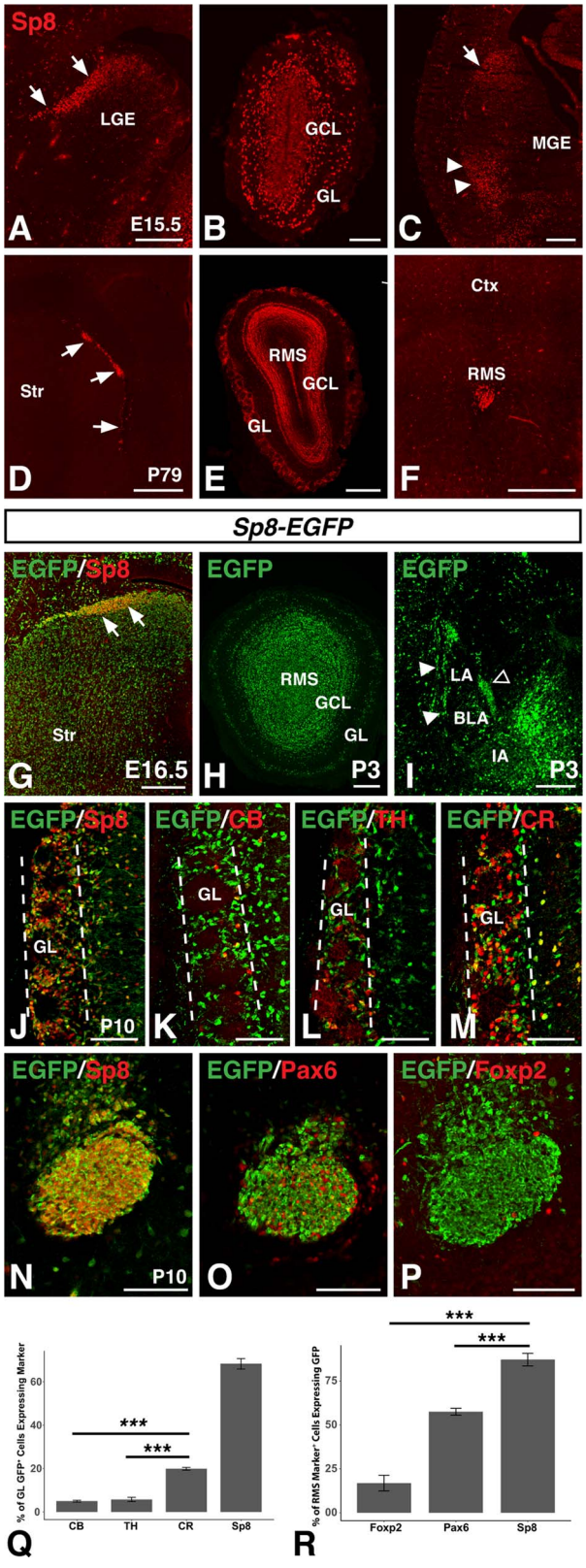

Figure 1. *Sp8*$^+$ progenitors differentially give rise to olfactory bulb interneurons. (*A–C*) Immunofluorescence showing Sp8 expression in the dLGE (arrows, *A*), GL and GCL of the olfactory bulb (*B*), and lateral migratory stream from the LGE (arrow) to the amygdala (arrowheads, *C*) at embryonic timepoints. (*D–F*) Immunofluorescence showing Sp8 expression in the SVZ along the lateral wall

development (Dellovade et al. 1998; Hack et al. 2005; Kohwi et al. 2005; Brill et al. 2008; Haba et al. 2009; Agoston et al. 2014; Fujiwara and Cave 2016). Consistent with a preferential role for Sp8 in the generation of CR^+ neurons, we found that whereas 87.2% of $Sp8^+$ cells in the RMS were $EGFP^+$ ($n = 4$) (Fig. 1N), significantly fewer Pax6 (57.5%; $n = 4$, $P = 5.1 \times 10^{-4}$) (Fig. 1O) or Foxp2 (16.9%; $n = 4$, $P = 4.6 \times 10^{-5}$) (Fig. 1P) expressing cells colabeled with EGFP (one-way ANOVA, $F_{(2,9)} = 102.9$, $P = 6.32 \times 10^{-7}$) (Fig. 1R). These results are in line with previous results suggesting that while Sp8 is widely expressed in the dLGE, it is not ubiquitous in OB interneuron precursors in the RMS (Waclaw et al. 2006). Thus, Sp8 expressing progenitors preferentially give rise to certain dLGE derived subpopulations (e.g., the CR^+ subpopulations) whereas others (CB^+) are likely to derive from Sp8 negative precursors.

Dlx5/6-tTA Driven Sp8 Misexpression

We next turned to a gain-of-function strategy to further characterize the effect of developmental Sp8 expression on subpallial neural progenitors. Previous work has shown that the transcription factors *Dlx5* and *Dlx6* are robustly expressed throughout the subpallial SVZ (Porteus et al. 1991; Price et al. 1991; Robinson et al. 1991; Simeone et al. 1994; Liu et al. 1997) and that a shared enhancer in the intergenic region between *Dlx5* and *Dlx6* is active in the progenitors that give rise to OB interneurons as well as the ITCs (Zerucha et al. 2000; Stenman et al. 2003a Allen et al. 2007; Waclaw et al. 2010). We generated a transgenic mouse line containing the tetracycline transactivator (*tTA*) (Gossen and Bujard 1992; Kistner et al. 1996) downstream of the *Dlx5/6*-enhancer (Zerucha et al. 2000) to drive transgene expression throughout the developing subpallium. To test the activity of this construct, we crossed *Dlx5/6-tTA* mice with a mouse line containing *IRES-EGFP* (*IE*) downstream of the tetO promoter (i.e., *tetO-IE* mice). *Dlx5/6-tTA;tetO-IE* double transgenic mice displayed robust EGFP expression in the ventral telencephalon (Fig. 2A). As expected, EGFP did not colocalize with the VZ marker Gsx2 (Fig. 2B) (Hsieh-Li et al. 1995; Toresson et al. 2000), but showed considerable overlap with Sp8 in the dLGE SVZ (Fig. 2C). Moreover, at late embryonic timepoints, EGFP expression was detected in structures derived from subpallial progenitors, namely the GL and GCL of the OB (Fig. 2D), the striatum (Fig. 2E) and in the ITCs of the amygdala as shown by the coexpression of Meis2 and Foxp2 (Fig. 2F). *Dlx5/6* enhancer activity has been reported in the SVZ of postnatal animals (Zerucha et al. 2000; Stenman et al. 2003a), and in line with this, we detected GFP expression in the postnatal RMS (Fig. 2G) and OB (Fig. 2H).

To manipulate Sp8 expression, we utilized a *tetO-Sp8-IRES-EGFP(IE)* transgene that can be temporally controlled by tTA and Dox administration (Borello et al. 2014). We utilized *Dlx5/6-tTA* transgenic mice to drive *Sp8* misexpression specifically throughout the subpallial SVZ (both dLGE and vLGE) by generating *Dlx5/6-tTA;tetO-Sp8-IRES-EGFP(IE)* double transgenic mice. In contrast to controls (i.e., *Dlx5/6-tTA* mice) which exhibited Sp8 expression in only the dLGE region (Fig. 2I), *Sp8* misexpressing embryos displayed Sp8 expression throughout the subpallial SVZ (Fig. 2J). In fact, the SVZ of these animals ($n = 4$) contained 20.7-fold more Sp8 expressing cells compared to that of controls ($n = 4$, $P = t_{(4.2)} = -33.0$, $P = 3.1 \times 10^{-6}$). Moreover, after Sp8 immunostaining, the fluorescence intensity within Sp8 expressing cells of *Sp8* misexpressing embryos ($n = 4$) was 1.7-fold stronger than those within the Sp8 expressing population of controls ($n = 4$, $t_{(3.3)} = -8.5$, $P = 2.3 \times 10^{-3}$), suggesting that Sp8 was both expressed in significantly more cells and at significantly higher levels in individual cells than in controls. Immunostaining for EGFP in the *Dlx5/6-tTA;tetO-Sp8-IE* embryos, revealed a similar pattern to the misexpressed Sp8 showing that EGFP expression can also be used to identify misexpressing *Sp8* cells (Fig. 2K).

Sp8 Misexpression Results in Increased ITC Numbers Via *Tshz1* Activation

Given that Sp8 is required for normal OB and ITC interneuron development (Waclaw et al. 2006, 2010; Li et al. 2018), we next set out to examine the effect of developmental Sp8 misexpression on LGE derived neuronal populations in postnatal mice. Immunostaining sections from P21 brains with the ITC markers Foxp2 and Meis2 (Stenman et al. 2003b; Takahashi et al. 2008; Kaoru et al. 2010; Waclaw et al. 2010; Kuerbitz et al. 2018) revealed a 52.5% increase in the number of ITCs in the *Sp8* misexpressing (i.e., *Dlx5/6-tTA; tetO-Sp8-IE*) animals (Fig. 3B) compared with *tetO-Sp8-IE* controls (Fig. 3A) ($n = 4$; $t_{(6)} = -12.8$, $P = 1.4 \times 10^{-5}$) (Fig. 3E). Notably, this increase was driven by increases in the lateral clusters (146% increase, $t_{(5.25)} = -16.0$, $p = 1.2 \times 10^{-5}$) and in the main intercalated mass (IA) (64.6% increase, $t_{(5.54)} = -4.87$, $p = 3.4 \times 10^{-3}$), whereas the medial ITC clusters were not affected significantly ($t_{(4.16)} = 2.04$, $p = 0.11$) (Fig. 3E). Additionally, immunohistochemistry for the mature ITC marker μOR (Kaoru et al. 2010; Waclaw et al. 2010) stained a 180% larger area within the amygdala of *Sp8* misexpressing animals (Fig. 3D) compared with controls (Fig. 3C) ($n = 4$; $t_{(6)} = -2.92$, $P = 0.027$) (Fig. 3F), consistent with increased ITC numbers.

Our recent work has shown that the zinc finger transcription factor *Tshz1* is essential for normal ITC development (Kuerbitz et al. 2018). Moreover, *Tshz1* may be a downstream target of Sp8 (Li et al. 2018). We performed in situ hybridization to determine if *Sp8* misexpression affected *Tshz1* expression levels in the LGE. *Sp8* misexpressing embryos ($n = 5$) exhibited a 2.02-fold increase in the area stained above background levels in the LGE by *Tshz1* antisense probe compared with controls (compare Fig. 4C with A; $n = 4$; $P = 0.014$; Fig. 4I). Interestingly, removing one *Tshz1* allele ($Tshz1^{RA/+}$) (Kuerbitz et al. 2018) was sufficient to reduce *Tshz1* levels in *Dlx5/6-tTA; tetO-Sp8-IE* embryos significantly (Fig. 4D) as compared with Sp8 misexpressing embryos possessing both *Tshz1* alleles (Fig. 4C) ($n = 6$, $P = 2.2 \times 10^{-3}$). Indeed, the *Tshz1* expression in

of the ventricle (*D*, arrows), GL, GCL, and RMS at olfactory bulb levels (*E*), and RMS (*F*) at adult timepoints. (*G–J*) The *Sp8-EGFP* BAC drives EGFP expression in the embryonic LGE (*G*, arrow) and marks *Sp8* derived populations in the olfactory bulb (*H*) and amygdala (*I*) at early postnatal timepoints as well as in Sp8 expressing GL cells at P10 (*J*). (*K–M*) In the olfactory bulb GL (between dashed lines) of postnatal *Sp8-EGFP* mice, 5.0% of GFP^+ cells express CB (*K*), 5.8% express TH (*L*), and 19.9% express CR (*M*). (*N–P*), in the postnatal RMS of *Sp8-EGFP* mice, 87.2% of $Sp8^+$ cells are $EGFP^+$ (*N*), 57.5% of $Pax6^+$ cells are $EGFP^+$ (*O*), and 16.9% of $Foxp2^+$ cells are $EGFP^+$ (*P*). (Q) Quantification of (*J–M*). (*R*) Quantification of (*N–P*). Data are expressed as mean ± SEM and stats performed using a one-way ANOVA followed by a post hoc Tukey HSD, $^{***}P < 0.001$. BLA, basolateral complex; IA, main intercalated mass; LA, lateral amygdala; LGE, lateral ganglionic eminence; GCL, granule cell layer; GL glomerular layer; MGE, medial ganglionic eminence; RMS, rostral migratory stream, Str, striatum; SVZ, subventricular zone. Scale bars: *A*, 200 μm; *B*, 100 μm; *C*, 250 μm; *D–F*, 500 μm; *G–I*, 200 μm; *J–P*, 100 μm.

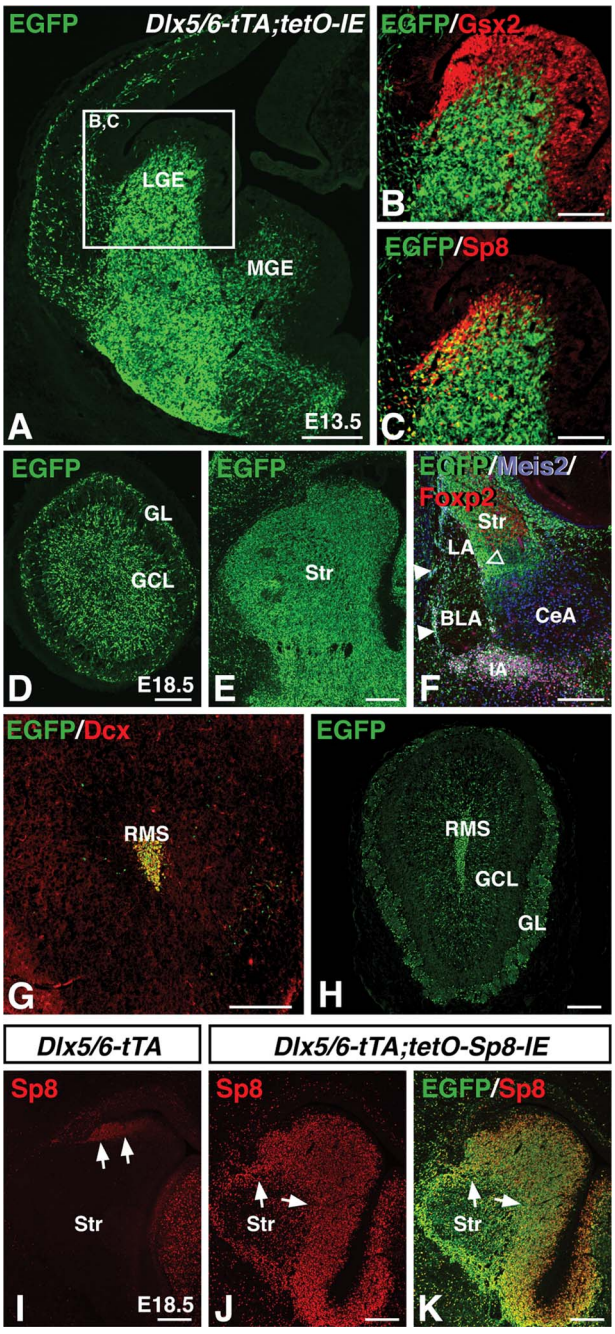

Figure 2. Misexpression of Sp8 throughout the subpallial SVZ using tTA driven from the Dlx5/6 enhancer. (*A*) *Dlx5/6-tTA* drives expression of the *tetO-IRES-EGFP(IE)* transgene throughout the SVZ and mantle regions of the LGE and MGE at embryonic timepoints. (*B*) EGFP transgene expression does not colocalize with the ventricular zone marker Gsx2. (*C*) colocalization of the dLGE SVZ marker Sp8 with transgene driven EGFP. (*D–F*) At E18.5, *Dlx5/6-tTA* driven EGFP expression can be detected in the GL and GCL of the olfactory bulb (*D*), striatum (Str) (*E*), and amygdala ITCs (which coexpress EGFP, Meis2, and Foxp2) (*F*). At adult timepoints, *Dlx5/6-tTA* continues to drive EGFP expression in Dcx^+ cells in the RMS (*G*), and olfactory bulb interneurons of the GCL and GL (*H*). (*I–K*) Crossing *Dlx5/6-tTA* mice with tetO-Sp8-IRES-EGFP(IE) mice results in misexpression of Sp8 throughout the SVZ and mantle region of the ventral telencephalon (*J*), as compared to the limited expression in the control dLGE (*I*). The IRES-EGFP leads to most Sp8 expressing cells coexpressing EGFP (*K*). BLA, basolateral amygdala; CeA, central amygdala; LGE, lateral ganglionic eminence; GCL, granule cell layer; GL glomerular layer; IA, main intercalated mass; LA, lateral amygdala; MGE, Medial ganglionic eminence; RMS, rostral migratory stream, SVZ, Subventricular zone. Scale bars: *A*, 250 µm; *B,C*, 125 µm; *D–F*, 200 µm; *G,H*, 250 µm; *I–M*, 200 µm.

the *Dlx5/6-tTA; tetO-Sp8-IE; Tshz1*$^{RA/+}$ embryos (Fig. 4D) was comparable to that seen in controls (Fig. 4A). This was revealed by a two-way ANOVA showing significant effects on *Tshz1* levels of both *Sp8* misexpression ($F_{(1,16)} = 9.6$, $P = 6.9 \times 10^{-3}$) and *Tshz1* heterozygosity ($F_{(1,16)} = 17.6$, $P = 6.9\text{x}10^{-4}$; Fig. 4I). This indicates that *Sp8* misexpression in LGE progenitors increases *Tshz1* gene expression in a manner dependent on *Tshz1* allele dosage.

We next set out to investigate whether alterations in *Tshz1* levels in *Sp8* misexpressing animals were accompanied by changes in ITC numbers. Immunostaining for Meis2 and Foxp2, showed that alterations in *Tshz1* levels in *Sp8* misexpressing embryos corresponded well with ITC number (Fig. 4E–H). In fact, a two-way ANOVA revealed significant effects of *Sp8* misexpression ($F_{(1,16)} = 17.0$, $P = 7.8 \times 10^{-4}$) and *Tshz1* heterozygosity ($F^{(1,16)} = 18.4$, $P = 5.6 \times 10^{-4}$) on total ITC number (Fig. 4J). Post hoc Tukey HSD testing revealed a significant (54.9%) increase in ITCs in *Sp8* misexpressing (i.e., *Dlx5/6-tTA; tetO-Sp8-IE*) embryos ($n = 5$) compared with controls ($n = 4$, $P = 0.011$). This increase was significantly abrogated by *Tshz1* heterozygosity (i.e., *Dlx5/6-tTA; tetO-Sp8-IE; Tshz1*$^{RA/+}$ embryos) ($n = 6$, $P = 5.4 \times 10^{-3}$), to levels comparable to controls.

Examination of the lateral ITC clusters, specifically, revealed a similar trend. Lateral ITC numbers were affected by *Sp8* misexpression (two-way ANOVA, $F_{(1,16)} = 23.0$, $P = 2.0 \times 10^{-4}$) and by *Tshz1* heterozygosity ($F_{(1,16)} = 21.6$, $P = 2.7 \times 10^{-4}$) (Fig. 4K). Indeed, lateral ITC numbers were 1.16-fold higher in *Sp8* misexpressing embryos as compared with controls ($P = 2.1 \times 10^{-3}$). This increase was reduced by *Tshz1* heterozygosity ($P = 1.5 \times 10^{-3}$) to control levels (Fig. 4K). Moreover we detected a significant correlation between *Tshz1* expression levels and total ITC counts (Pearson coefficient = 0.72, $t_{(18)} = 4.4$, $P = 3.4 \times 10^{-4}$) (Fig. 4L) as well as between *Tshz1* expression levels and lateral ITC counts (Pearson coefficient = 0.75, $t_{(18)} = 4.8$, $P = 1.5 \times 10^{-4}$) (Fig. 4M). Together, these results suggest that *Sp8* misexpression is sufficient to increase *Tshz1* expression levels and that Sp8 promotes increased ITC numbers within the paracapsular amygdala regions in a *Tshz1*-dependent manner.

Misexpression of Sp8 Results in Reduced Numbers of TH^+ and CB^+ OB Interneurons

Next, we investigated the effect of *Sp8* misexpression on the other dLGE derived neuronal populations, namely the OB interneurons. *Sp8* misexpression did not produce significant alterations in the number of CR^+ interneurons observed in the GL at postnatal timepoints (P21) (Fig. 5A–C). On the other hand, *Sp8* misexpressing animals showed dramatic reductions in the density of TH^+ cells (−43.9%, $n = 5$, $t_{(8)} = 2.6$, $P = 3.0 \times 10^{-2}$) (Fig. 5D–F) and CB^+ cells (−63.7%, $n = 4$, $t_{(6)} = 5.1$, $P = 2.2 \times 10^{-3}$) (Fig. 5G–I) observed in the GL compared with *tetO-Sp8* controls. Foxp2 has been reported to mark CB^+ OB interneurons (Fujiwara and Cave 2016), and we detected a similar 47.7% reduction in $Foxp2^+$ cells in the GL of *Sp8* misexpressing animals compared with controls ($n = 4$, $t_{(6)} = 7.9$,$P = 2.3 \times 10^{-4}$) (Fig. 5J–L). Meis2 has been reported to generally colocalize with OB interneurons expressing CR, TH, or CB (Allen et al. 2007; Agoston et al. 2014). Immunostaining for Meis2 revealed a significant (−29.8%) decrease in $Meis2^+$ interneurons ($n = 4$, $t_{(6)} = 7.1$, $P = 4.0 \times 10^{-4}$) (Fig. 5M–O), although it was less pronounced than the reduction observed in Foxp2, consistent with the CR^+ population being relatively unaffected. This indicates that misexpression of Sp8 preferentially results in reduced numbers of the TH^+

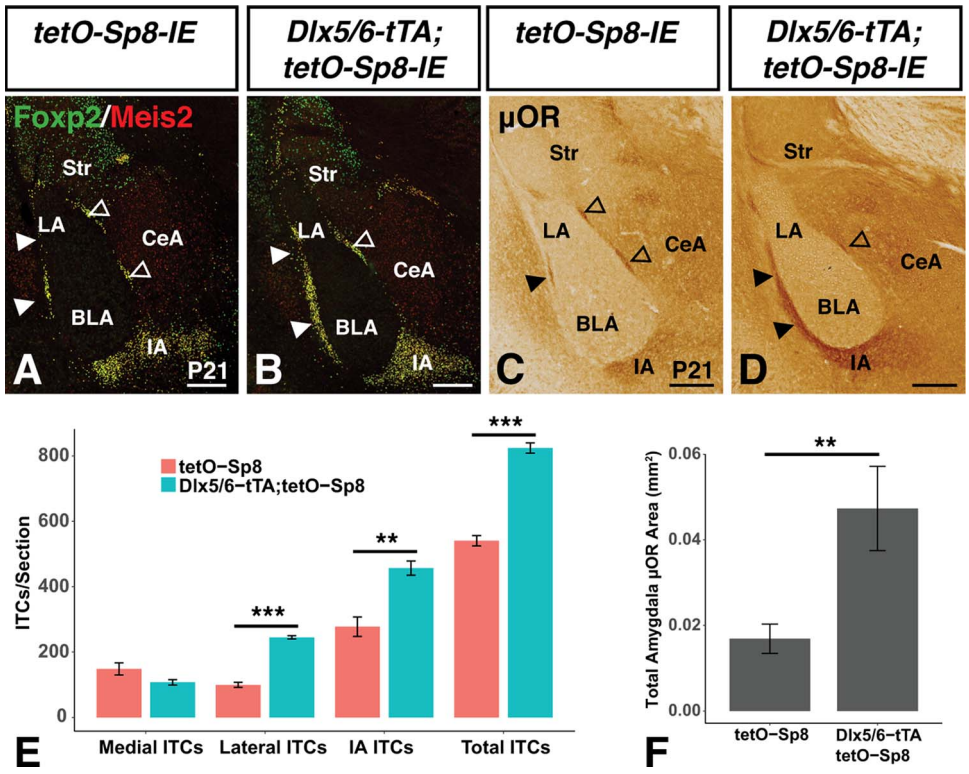

Figure 3. *Sp8* misexpression promotes increased numbers of ITCs within the amygdala. (*A*,*B*) *Sp8* misexpressing (i.e., *Dlx5/6-tTA;tetO-Sp8-IE*) mice show increased numbers of ITCs in the lateral clusters and IA as marked by Foxp2 and Meis2 expression when compared to controls (i.e., *tetO-Sp8-IE*). (C,D) μOR expression demonstrates ITC increases in the amygdala of *Sp8* misexpressing mice. (*E*) Quantification of *A* and *B* using a two-way ANOVA followed by a post hoc Tukey HSD, $^{**}P < 0.01$, $^{***}P < 0.001$. (*F*) Quantification of *C* and *D* using a Students's *t*-test, $^{**}P<0.01$. Data are represented as mean ± SEM. BLA, basolateral amygdala; CeA, central amygdala; IA, main intercalated mass; LA, lateral amygdala; Str, striatum. Scale bars: *A*–*D*, 250 μm.

and $CB^+/Foxp2^+$ populations of OB GL interneurons. We next examined whether *Tshz1* contributed to the altered OB interneuron numbers in the *Sp8* misexpressing animals. Removal of one allele of *Tshz1* actually significantly improved the number of $Foxp2^+$ (i.e., CB) GL neurons in the OBs of Sp8 misexpressing mice (Supplementary Fig. 1A–E). A two-way ANOVA revealed significant effects of *Sp8* misexpression ($F_{(1,8)} = 43.6$, $P = 1.7 \times 10^{-4}$) and the *Sp8* mixespression:*Tshz1* heterozygosity interaction ($F^{(1,8)} = 19.9$, $P = 2.1 \times 10^{-3}$) on total GL $Foxp2^+$ cells. Post hoc Tukey HSD testing revealed a significant (45.0%) decrease in GL $Foxp2^+$ cells in *Sp8* misexpressing (i.e., *Dlx5/6-tTA; tetO-Sp8-IE*) embryos ($n = 3$) compared with controls ($n = 3$, $P = 2.4 \times 10^{-4}$). This decrease was significantly abrogated by *Tshz1* heterozygosity (i.e., *Dlx5/6-tTA; tetO-Sp8-IE; Tshz1*$^{RA/+}$ embryos) ($n = 3$, $P = 8.7 \times 10^{-3}$). Interesting, similar assessment of the $Meis2^+$ population (Supplementary Fig. 1F–J) revealed an *Sp8* effect ($F_{(1,8)} = 14.8$, $P = 4.8 \times 10^{-3}$) but no *Tshz1* effect ($F_{(1,8)} = 0.72$, $P = 0.42$) or interaction ($F_{(1,8)} = 0.62$, $P = 0.45$).These findings suggest that *Tshz1* gene dosage differentially regulates the number of $Foxp2^+$ ITCs versus $Foxp2^+$ (i.e., CB) OB interneurons, downstream of Sp8.

To examine whether Sp8 misexpression alters the development of interneurons within the GCL, we quantified the numbers of $Meis2^+$ GCL neurons and found that no significant difference was apparent between the control ($n = 4$) and Sp8 misexpressing mice ($n = 4$) (Supplementary Fig. 2). Although Meis2 is not an exclusive marker of the GCL interneurons, it marks a very large number of these neurons and thus it appears that *Sp8* misexpression does not cause overt disruptions in the formation of this OB layer.

Interestingly, the SVZ of *Sp8* misexpressing mice frequently appeared expanded and disorganized (Fig. 5P,Q). Additionally, *Sp8* misexpressing animals displayed clusters of CR^+ expressing cells in the SVZ (Fig. 5Q) that were not evident in those of controls (Fig. 5P). In fact, the number of CR^+ cells located in the SVZ was increased by 18.5-fold compared with controls ($n = 4$, $t_{(3.05)} = -3.3$, $P = 0.043$) (Fig. 5R). Given that Sp8 has previously been suggested to facilitate CR^+ interneuron development (Waclaw et al. 2006), we interpreted this buildup of CR^+ cells in the postnatal germinal zone in the absence of a significant reduction in OB CR^+ cell levels to suggest that elevated levels of Sp8 may lead to increased generation of CR^+ interneurons but simultaneously disrupt at least a portion of these misexpressing cells along their migratory path. As mentioned earlier, Sp8 is also known to be required for the normal numbers of PV^+ neurons in the EPL of the OB (Li et al. 2011). Interestingly, we found that PV^+ EPL neurons were significantly reduced (−57.0%) in the *Sp8* misexpressing mice ($n = 3$, $t_{(4)} = 4.9$, $P = 8.2 \times 10^{-3}$, Supplementary Fig. 3). Unlike the case with CR^+ interneurons, however, we did not observe PV^+ cells clumped within the SVZ/RMS. It remains possible, however, that the $Sp8^+$ cells destined to generate PV^+ neurons may also be disrupted

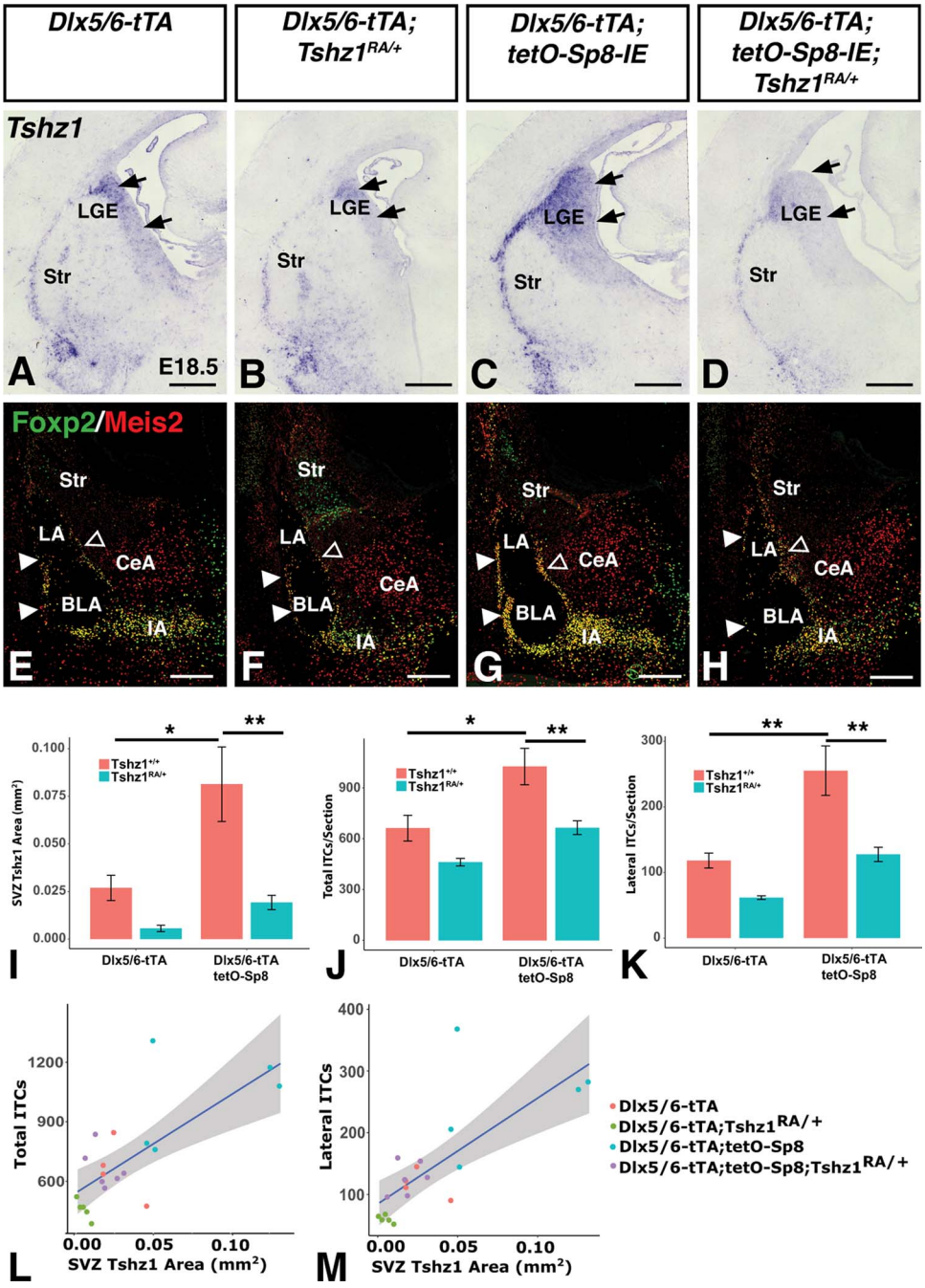

Figure 4. *Sp8*-induced increase in ITC numbers is dependent on Tshz1 gene dosage. (*A–D*), *Sp8* misexpressing mice (*Dlx5/6-tTA;tetO-Sp8-IE*, *C*) show expanded *Tshz1* expression in the LGE SVZ (arrows) as well as in the lateral migratory stream toward the amygdala when compared to controls (*A*). *Tshz1* heterozygosity ($Tshz1^{RA/+}$) results in reduced *Tshz1* expression in *Sp8* misexpressing mice (*D*) as well as the *Dlx5/6-tTA* controls (*B*). (*E–H*) Furthermore, *Sp8* misexpressing mice show increases in total and lateral ITC (marked by Foxp2/Meis2) numbers (*G*) as compared to controls (*E*). *Tshz1* heterozygosity in *Sp8* misexpressing mice restores ITC numbers to control levels (compare *H* with *E*). (*I*) Quantification of *Tshz1* expression area from (*A*) to (*D*). J, Quantification of total ITCs from (*E*) to (*H*). (*K*) Quantification of lateral ITCs from (*E*) to (*H*). Data are represented as mean ± SEM and stats were performed using a two-way ANOVA with a post hoc Tukey HSD, $^{*}P < 0.05$, $^{**}P < 0.01$. (*L*) Correlation between total ITC number and *Tshz1* expression area from (*A*) to (*H*). (*M*) Correlation between lateral ITC number and *Tshz1* expression area from (*A*) to (*H*). BLA, basolateral amygdala; CeA, central amygdala; IA, main intercalated nucleus of the amygdala; ITCs, intercalated cells; LA, lateral amygdala; LGE, lateral ganglionic eminence; Str, striatum; SVZ, subventricular zone. Scale bars: A-D, 250 µm; E-H, 200 µm.

along their migratory path similar to the CR^{+} interneurons but unable to differentiate into the PV subtype due to sustained Sp8 expression.

To determine whether high levels of Sp8 might interfere with the generation and/or migration of OB interneurons, we examined the OBs of *Sp8* misexpressing animals at late embryonic timepoints, using developmental transcription factors to mark distinct populations of immature interneurons. *Sp8* misexpressing embryos ($n = 4$) displayed a striking reduction in GL densities of all embryonic interneuron markers examined

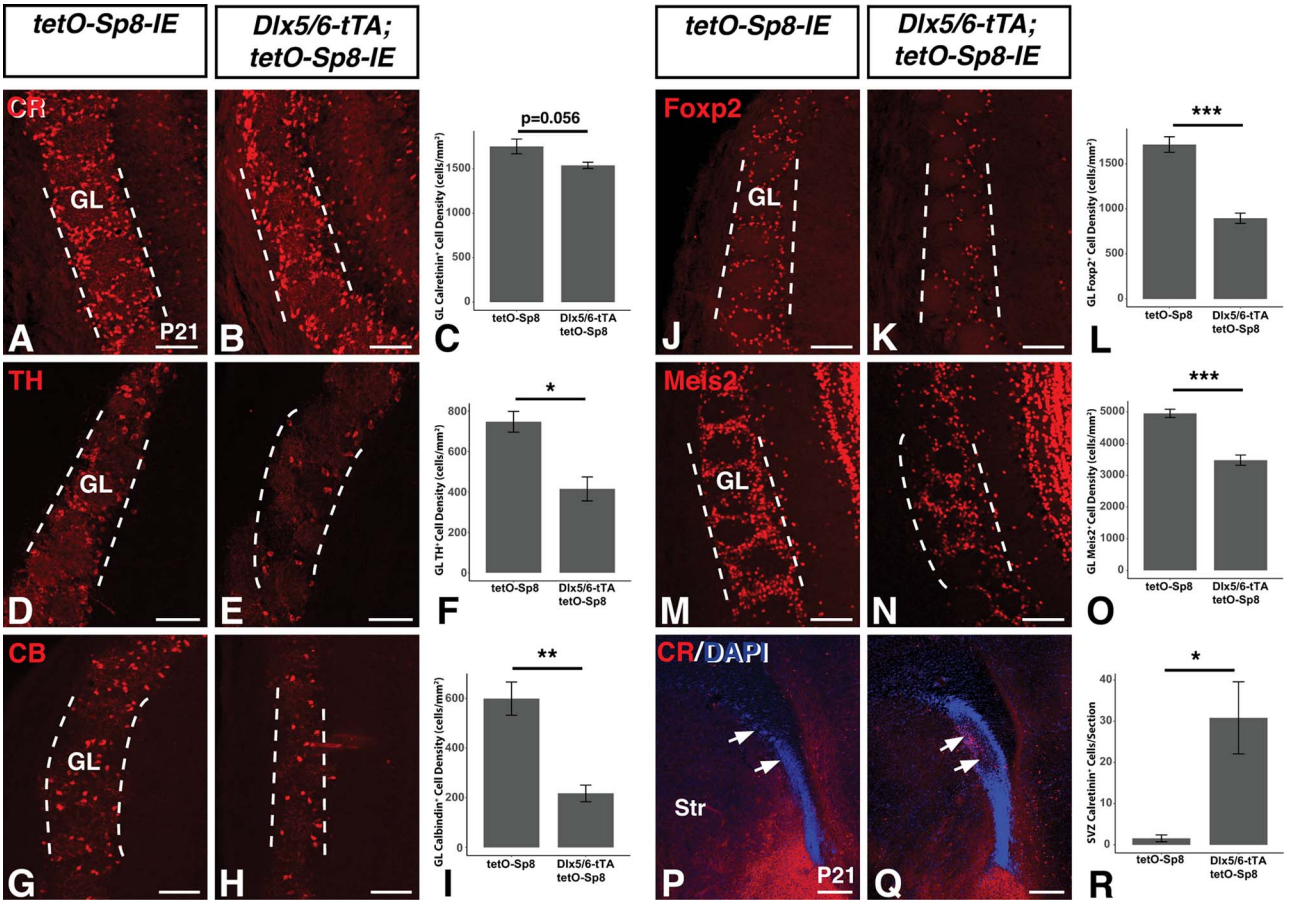

Figure 5. *Sp8* misexpressing mice exhibit reductions in TH and CB expressing OB GL interneurons. (*A–C*) Immunofluorescence (*A,B*) and quantification (*C*) of CR expressing neurons in the postnatal olfactory bulb GL (between dashed lines) of *Sp8* misexpressing mice which showed no significant effect. (*D–F*) Immunofluorescence (*D,E*) and quantification (*F*) of TH expressing neurons in the postnatal olfactory bulb GL (between dashed lines) of *Sp8* misexpressing mice reveals a 43.9% decrease in TH^+ cell density compared to controls. (*G–I*) Immunofluorescence (G,H) and quantification (*I*) of CB expressing neurons in the postnatal olfactory bulb GL (between dashed lines) of *Sp8* misexpressing mice reveals a 63.8% decrease in CB^+ cell density compared to controls. (*J–L*) Immunofluorescence (*J,K*) and quantification (*L*) of Foxp2 expressing neurons in the postnatal olfactory bulb GL (between dashed lines) of *Sp8* misexpressing mice reveals a 47.8% decrease in $Foxp2^+$ cell density compared to controls. (*M–O*) Immunofluorescence (*M,N*) and quantification (O) of Meis2 expressing neurons in the postnatal olfactory bulb GL (between dashed lines) of *Sp8* misexpressing mice reveals a 29.8% decrease in $Meis2^+$ cell density compared to controls. (*P–R*) Immunofluorescence (*P,Q*) and quantification (*R*) of CR expressing neurons in the postnatal SVZ of *Sp8* misexpressing mice reveals an 18.5-fold increase in CR^+ cells (arrows) compared to controls. Data are represented as mean ± SEM and stats performed using a Student's t-test, $^*P<0.05$, $^{**}P<0.01$, $^{***}P<0.001$. GL, glomerular layer, Str, striatum. Scale bars: *A–N*, 100 µm; *P,Q*, 250 µm.

compared with controls ($n=4$) (Fig. 6A). Foxp2 density was reduced by 51.1% ($t_{(6)}=3.0$, $P=0.024$), Meis2 density by 56.7% ($t_{(6)}=5.9$, $P=1.1\times10^{-3}$), and Pax6 density by 55.6% ($t_{(6)}=3.7$, $P=9.5\times10^{-3}$). Interestingly, despite being overexpressed, the density of $Sp8^+$ cells was not significantly increased and indeed appeared reduced ($t_{(3.1)}=2.63$, $P=0.063$). We took this in conjunction with the general reduction in other developmental interneuron markers to suggest that misexpression of Sp8 interferes with the normal generation and/or migration of olfactory interneurons prior to their reaching the OB.

Next, we compared the GL density of *Dlx5/6-tTA* driven *Sp8* misexpressing cells, marked by EGFP in *Dlx5/6-tTA;tetO-Sp8-IE* embryos, to that in the *Dlx5/6-tTA* expressing lineage, marked by EGFP in *Dlx5/6-tTA;tetO-IE* embryos. *Dlx5/6-tTA;tetO-Sp8-IE* embryos ($n=4$) displayed a 56.5% reduction in the density of $EGFP^+$ cells in the GL compared with *Dlx5/6-tTA;tetO-IE* (i.e., control) embryos ($n=3$, $t_{(2.2)}=5.2$, $P=0.028$), consistent with impairment of OB interneuron generation, survival and/or neuronal migration by misexpression of Sp8 (Fig. 6B–D).

To study the fate of Sp8 overexpressing neuroblasts, we compared the expression of developmental markers in $EGFP^+$ cells between *Dlx5/6-tTA;tetO-Sp8-IE* embryos and *Dlx5/6-tTA;tetO-IE* controls. As expected, we found that $EGFP^+$ GL cells in *Sp8* misexpressing embryos ($n=3$) were 46.5% more likely to express Sp8 than EGFP labeled cells in controls ($n=3$, $t_{(4.4)}=-3.2$, $P=0.028$) (Fig. 6E–I). Pax6 has previously been shown to play a crucial role in the generation of TH^+ interneurons (Hack et al. 2005; Kohwi et al. 2005; Brill et al. 2008). The number of $EGFP^+$ GL cells also expressing Pax6 in Sp8 misexpressing embryos ($n=4$) appeared slightly lower but was not significantly different from controls ($n=3$, $t_{(4.8)}=1.7$, $P=0.14$) (Fig. 6J–N). Foxp2 has previously been shown to be specifically expressed in CB interneurons in the mouse OB (Fujiwara and Cave 2016), and in accordance with this, $EGFP^+$ GL cells of Sp8 misexpressing embryos ($n=4$) were far less likely (−87.1%) to be positive for Foxp2 than EGFP cells in controls ($n=3$, $t_{(4.4)}=4.38$, $P=0.038$) (Fig. 6O–S). Interestingly, $EGFP^+$ GL cells in Sp8 misexpressing embryos ($n=4$) showed a 67.6% increase in the expression of the interneuron marker

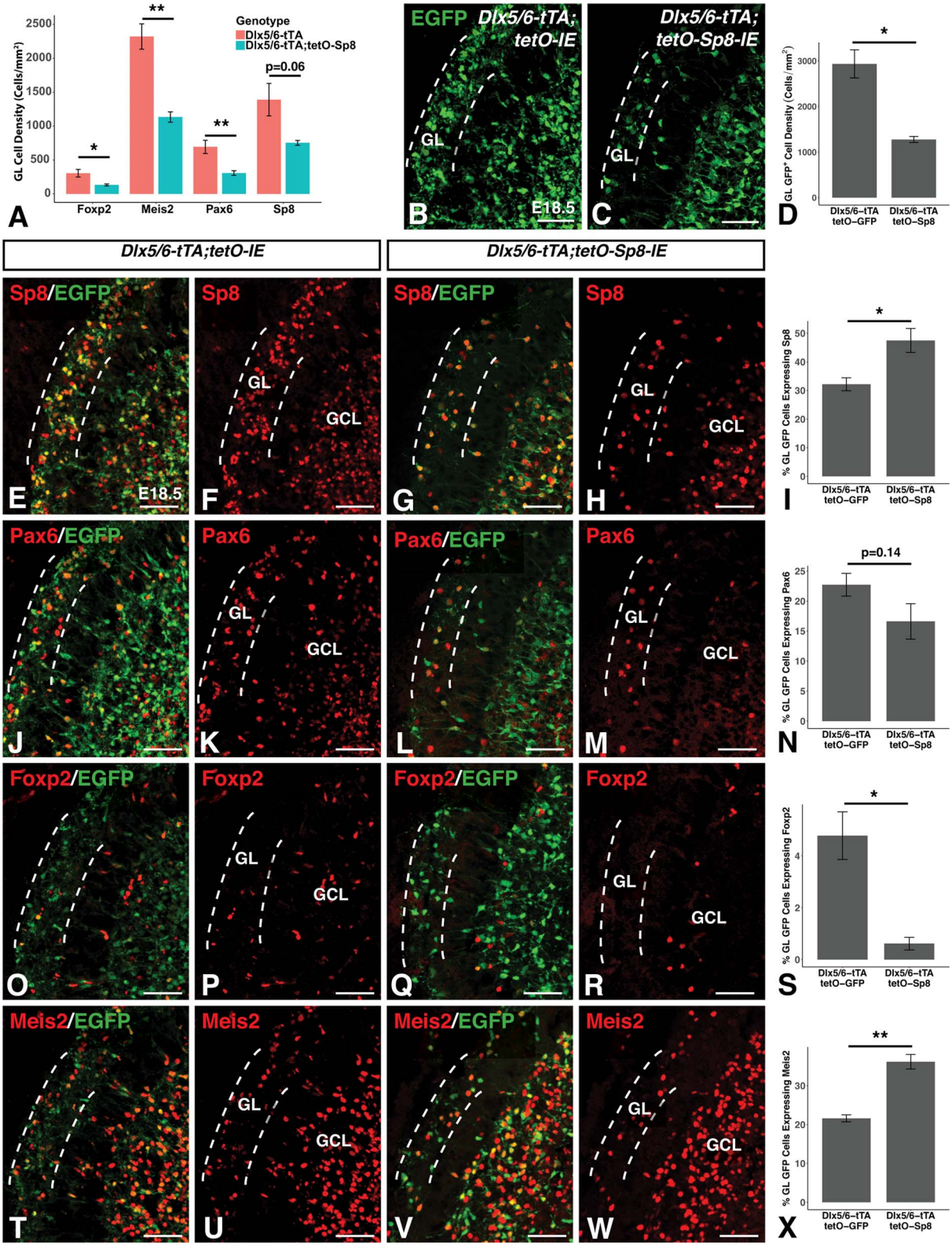

Figure 6. *Sp8 misexpression reduces OB GL interneuron numbers and inhibits Foxp2 expression.* (A) Quantification of developmental interneuron markers reveals reductions in Foxp2$^+$, Meis2$^+$ and Pax6$^+$ cell density in the olfactory bulb GL at late embryonic timepoints (Foxp2: −56.7%, Meis2: −51.1%, Pax6: −55.6%). A nonsignificant trend toward a 45.8% reduction in Sp8$^+$ cells as recorded. (*B–D*) Immunofluorescence (*B*,*C*) and quantification (*D*) showing reduced EGFP$^+$ cell density in the GL (between dashed lines) of *Sp8* misexpressing mice (*C*) compared to EGFP-expressing controls (*B*) recorded as a 56.5% reduction (*D*). (*E–I*) Immunofluorescence (*E–H*) and quantification (*I*) showing 46.5% increased Sp8 coexpression in EGFP$^+$ GL cells of *Sp8* misexpressing mice (*G*,*H*) compared to controls (*E*,*F*). (*J–N*) Immunofluorescence (*J–O*) and quantification (*N*) showing a nonsignificant trend toward a reduction in Pax6 coexpression in EGFP$^+$ cells in the GL of *Sp8* misexpressing (*L*,*M*) mice compared to EGFP-expressing controls (*J*,*K*). (*O–S*) Immunofluorescence (*O–R*) and quantification (*S*) showing an 87.1% reduction in Foxp2 coexpression in EGFP$^+$ cells in the GL of *Sp8* misexpressing mice (*Q*,*R*) compared to controls (*O*,*P*). (*T–X*) Immunofluorescence (*T–W*) and quantification (*X*) showing a 67.6% increase in Meis2 coexpression in EGFP$^+$ cells in the GL of *Sp8* misexpressing mice (*V*,*W*) compared to EGFP-expressing controls (*T*,*U*). Data are represented as mean ± SEM and stats were performed using a Student's *t*-test, $^{**}P < 0.01$, $^{*}P < 0.05$. GL, glomerular layer; GCL, granule cell layer. Scale bars: 50 µm.

Meis2 compared to the EGFP cells observed in controls ($n = 3$, $t_{(4.22)} = -7.0$, $P = 0.002$) (Fig. 6T–X), suggesting that *Sp8* misexpressing cells that reached the OB retained certain aspects of OB interneuron identity but were less likely to express markers characteristic of a TH^+ or CB^+ identity (Allen et al. 2007; Agoston et al. 2014).

Sp8 Misexpression Suppresses vLGE Fates

Embryonic Sp8 expression defines the dLGE in wild-type mice (Waclaw et al. 2006), but in *Dlx5/6-tTA;tetO-Sp8-IE* embryos Sp8 is expanded into the vLGE, the embryonic source of SPNs (Stenman et al. 2003a, Ehrman et al. 2013), at early developmental timepoints (see e.g., Fig. 2J,K). Therefore, we next analyzed the striatum in *Sp8* misexpressing animals to investigate if forced Sp8 expression in the vLGE affected the development of the striatum using Foxp1 as a marker of SPNs (Tamura et al. 2004; Precious et al. 2016). Already at E18.5, *Sp8* misexpressing embryos exhibited a 41.3% reduction in striatal cross-sectional Foxp1-stained area ($n = 4$, $t_{(6)} = 7.0$, $P = 4.3710^{-4}$) (Fig. 7A–C) as well as a 51.1% reduction in the number of $Foxp1^+$ nuclei observed per section ($n = 4$, $t_{(6)} = 6.7$, $P = 5.2010^{-4}$) (Fig. 7D). Foxp2 is also expressed in cells of the LGE SVZ and striatum (Takahashi et al. 2008). Accordingly, we found a significant 42.4% reduction in $Foxp2^+$ SPNs of the misexpressing mice ($n = 4$, $t_{(6)} = 3.7$, $P = 9.9 \times 10^{-3}$) together with a nonsignificant trend toward an increase in $Foxp2^+$ cells within the SVZ of the LGE ($n = 4$, $t_{(6)} = -2.1$, $P = 0.079$, Supplementary Fig. 4). At P21, a similar phenotype was apparent with significant reductions in both the striatal size and the number of $Foxp1^+$ SPNs (Fig. 7E,F). The cross-sectional area of the striatum (as marked by the area occupied by the mature SPN marker Darpp-32, Anderson and Reiner 1991) in coronal sections was 44.0% lower in *Sp8* misexpressing animals compared with *tetO-Sp8* controls ($n = 4$, $t_{(6)} = 6.9$, $P = 4.68 \times 10^{-4}$) (Fig. 7G) at postnatal timepoints. Additionally, the number of $Foxp1^+$ SPNs was reduced by 48.4% in *Sp8* misexpressing mice ($n = 4$, $t_{(6)} = 8.7$, $P = 1.24 \times 10^{-4}$) (Fig. 7H). *Tshz1* gene dosage did not appear to affect the striatal phenotype observed in *Sp8* misexpressing mice ($F^{(1,8)} = 1.5$, $P = 0.26$, Supplementary Fig. 1K–O).

Given the loss of striatal neurons and increased ITC numbers in Sp8 misexpressing animals, we wondered whether vLGE progenitors misexpressing Sp8 were respecified toward an ITC fate. To address this question, we used $Isl1^{cre}$ mice to specifically express *Sp8* in vLGE progenitors via a $Rosa^{tTA}$ driver (Wang et al. 2008; Ehrman et al. 2013). In these mice, cre expression leads to activation of the tetO promoter by excising a stop cassette from the *ROSA26* locus and activating tTA expression. To permanently label cells derived from the *Isl1* lineage we used the cre-inducible $Rosa^{tdTomato(Tom)}$ allele (Ai14) (Madisen et al. 2010). Analysis of 57 animals between ages E15.5 and P0.5 across 8 litters produced no Sp8 misrexpressing animals whereas several misrexpressing embryos were obtained at E11.5, suggesting that Sp8 misexpression in the *Isl1* lineage likely induces lethality between E11.5 and E15.5. To circumvent this difficulty, we resorted to a tamoxifen inducible $Isl1^{CreER}$ allele (Laugwitz et al. 2005) and gave 2 does of tamoxifen; one at E11.5 and another at E13.5 and collected pups at E17.5. As expected, striatal neurons exhibited robust Tomato expression in control animals ($Isl1^{CreER}$;$Rosa^{tdTom/+}$;*tetO-Sp8-IE*) (Fig. 7I). Robust Tomato expression was also observed in $Isl1^{CreER}$; $Rosa^{tdTom/tTA}$; *tetO-Sp8-IE* mice (Fig. 7J), however, only a small number of Tomato labeled cells coexpressed Sp8 in these animals (Fig. 7J). Accordingly, the size of the striatum was not obviously different between the $Isl1^{CreER}$;$Rosa^{tdTom/+}$;*tetO-Sp8-IE* and $Isl1^{CreER}$;$Rosa^{tdTom/tTA}$;*tetO-Sp8-IE* mice. Despite the limited number of striatal (i.e., vLGE) cells observed to misexpress Sp8, we would expect that if these cells are being respecified toward ITC fates and altering their migration toward the LMS, we would observe some $Tomato^+$ cells within the ITC clusters of the $Isl1^{CreER}$;$Rosa^{tdTom/tTA}$;*tetO-Sp8-IE* amygdala. In control ($Isl1^{CreER}$;$Rosa^{tdTom/+}$;*tetO-Sp8-IE*) animals ($n = 3$), no $Tomato^+$ cells were observed within ITC clusters (Fig. 7K arrowheads) while significant overlap was observed with $Foxp2^+$ SPNs (arrows), as expected. Moreover, $Tomato^+$ labeled cells were also never identified within the ITC clusters of the $Isl1^{CreER}$;$Rosa^{tdTom/tTA}$;*tetO-Sp8-IE* amygdala ($n = 3$), suggesting that Sp8 misexpression in vLGE progenitors (e.g., the *Isl1* lineage) is not capable of redirecting these progenitors toward an ITC destination (Fig. 7L). Finally, the *Isl1* vLGE lineage also provides projection neurons to the CeA (Waclaw et al. 2010) and these neurons are $Tomato^+$ in the Isl1 fate-mapped animals (Fig. 7K,L). Notably, the size of the CeA was not obviously different between the Sp8 misexpressing animals and controls, likely due to the limited numbers of fate-mapped cells that misexpress Sp8.

Distinct Temporal Windows of Sp8 Sensitivity in LGE Progenitors

To study the importance of temporal regulation of Sp8 activity for the control of LGE neuron development, we used Dox treatment to suppress tTA activity by administering Dox in drinking water of the pregnant dams. Since the *Dlx5/6-tTA* mice are a new tool for inducible gene expression studies, we tested each of our previous Dox protocols developed for the $Foxg1^{tTA}$ mice (Waclaw et al. 2009; Pei et al. 2011; Chapman et al. 2013; Borello et al. 2014). We found that adding Dox from E7 to E11 (Fig. 8A) was sufficient to suppress *tetO* driven transgene expression (i.e., Sp8 and EGFP) in *Dlx5/6-tTA;tetO-Sp8-IE* mice at E13.5 (Fig. 8B–D). By E15.5, Dox-treated mice exhibited robust transgene expression in the LGE, whereas EGFP/Sp8 expressing cells were rarely observed in the striatum (Fig 8E–G). Finally, at E18.5, robust Sp8 and EGFP expression could be observed in both the SVZ and striatum of Dox-treated mice (Fig 8H–J). Thus, it appears that the E7–E11 Dox protocol results in delayed *tetO*-driven transgene expression until around E14–15 using the *Dlx5/6-tTA* mice.

To determine the effect of *Sp8* overexpression at early timepoints (e.g., up to E14) versus late embryonic timepoints (i.e., E14 onward), we analyzed the brains of P21 *Sp8* misexpressing animals following Dox treatment from E7 to E11. Dox treatment was sufficient to completely reverse the increases in lateral ITC numbers in *Sp8* misexpressing mice (Fig. 9A–E). A two-way ANOVA revealed significant effects of the interaction between *Sp8* misexpression and Dox treatment ($F_{(1,8)} = 16.62$, $P = 3.55 \times 10^{-3}$). *Sp8* misexpressing mice ($n = 5$) treated with Dox displayed a 58.1% reduction in lateral ITCs compared with untreated *Sp8* misexpressing mice ($n = 3$, $P = 1.18 \times 10^{-3}$) and were comparable to control mice ($n = 3$). Thus, it appears that LGE progenitors are sensitive to Sp8 misexpression to increase the numbers of amygdala ITCs only between E12 and E15.

In contrast to this result, Dox treatment did not produce a complete reversal of the reduction in $Foxp2^+$ cells in the OB of *Sp8* misexpressing mice (Fig. 9F–J). A two-way ANOVA revealed a significant effect of *Sp8* misexpression ($F_{(1,8)} = 28.1$, $P = 7.28 \times 10^{-4}$) as well as an effect of Dox treatment ($F_{(1,8)} = 8.36$, $P = 0.02$). Pairwise comparisons with post hoc Tukey HSD tests revealed that *Sp8* misexpressing mice ($n = 5$) treated with Dox

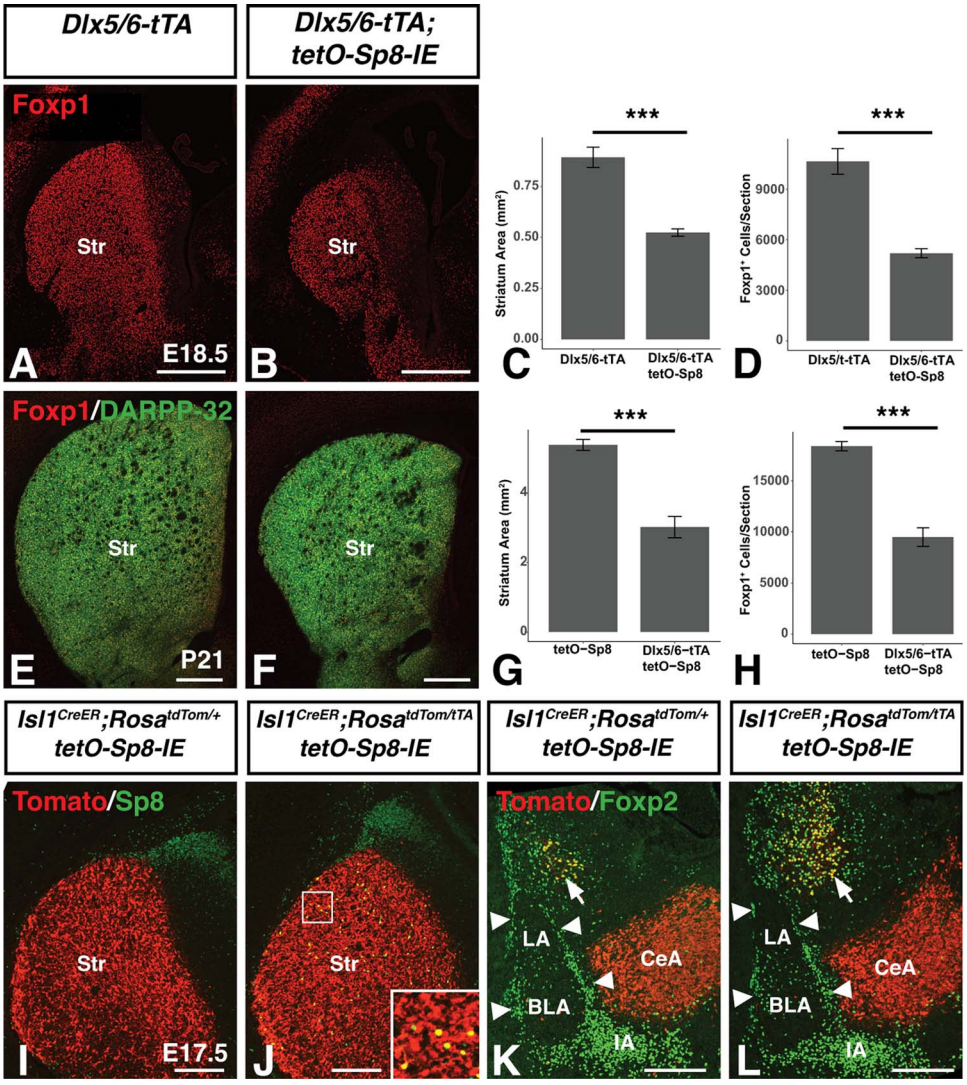

Figure 7. Reduced striatal size in Sp8 misexpressing mice. (*A–D*), Immunofluorescence (*A,B*) and quantification illustrating a 44.0% reduced cross-sectional striatal area (*C*) and 48.4% reduction in Foxp1$^+$ SPNs (*D*) in late embryonic (i.e. E18.5) *Sp8* misexpressing mice as compared to controls. (*E–H*) Immunofluorescence (*E,F*) and quantification illustrating a 41.3% reduced cross-sectional striatal area (*G*) and a 51.2% reduction in Foxp1$^+$ SPNs (*H*) adult (i.e. P21) *Sp8* misexpressing mice compared to controls. Data are represented as mean ± SEM and stats were performed using a Student's t-test, $^{***}P<0.01$. *I*, *Isl1^{creER};Rosa$^{tdTom/+}$;tetO-Sp8* mice exhibit robust tomato labeling of the striatum following tamoxifen injection on days E11.5 and E13.5. (*J*) *Isl1^{CreER};Rosa$^{tdTom/tTA}$;tetO-Sp8* mice also exhibit robust tomato labeling of the striatum with only a limited number of recombined cells expressing high levels of Sp8 (yellow cells in inset). (*K,L*) Ventral (v)LGE progenitors marked by the *Islet1^{creER}* fate-mapped cells are not observed in the ITC clusters (arrowheads) or IA in controls (*K*) as expected. Moreover, we did not observe Isl1 fate-mapped cells in the ITC clusters of Sp8 misexpressing embryos (*L*). Str, Striatum. Scale bars: *A,B,E,F*, 500 µm; *I–L*, 200 µm.

did not have significantly more Foxp2$^+$ GL cells than did untreated *Sp8* misexpressing mice ($n=3$, $P=0.12$). Additionally, whereas Dox-treated *Sp8* misexpressing animals did not have significantly fewer Foxp2$^+$ GL cells than controls ($n=3$), the difference (24.8%) approached statistical significance ($P=0.051$).

Finally, Dox-mediated delay of *Sp8* misexpression rescued the striatal phenotype in *Sp8* misexpressing mice (Fig. 9K–O). A two-way ANOVA revealed significant effects of the interaction between *Sp8* misexpression and Dox treatment ($F_{(1,8)}=30.3$, $P=5.69\times10^{-4}$) on striatal area. Following Dox treatment, *Sp8* misexpressing animals ($n=5$) exhibited a 38.1% increase in striatal volume compared with untreated *Sp8* misexpressing animals ($n=3$, $P=3.6\times10^{-4}$), and their striatum size was similar to that of controls ($n=3$). These findings suggest that vLGE progenitors are sensitive to ectopic Sp8 expression only between E12 and E15, while the Foxp2$^+$/CB$^+$ GL interneurons remain susceptible even after E15. These findings are in line with the fact that SPNs and ITCs are specified at early embryonic stages (Waclaw et al. 2009) and the OB interneurons begin to arise at later embryonic stages (Hinds 1968; Tucker et al. 2006) with the majority generated at postnatal stages (Hinds 1968; Luskin 1993; Lois and Alvarez-Buylla 1994).

Discussion

Progenitors within the ganglionic eminences are molecularly heterogeneous, and this heterogeneity relates to the types of mature neurons that are generated from particular subdomains and from individual cells (Lledo et al. 2008; Mayer et al. 2018). The present work extends our understanding of the role of

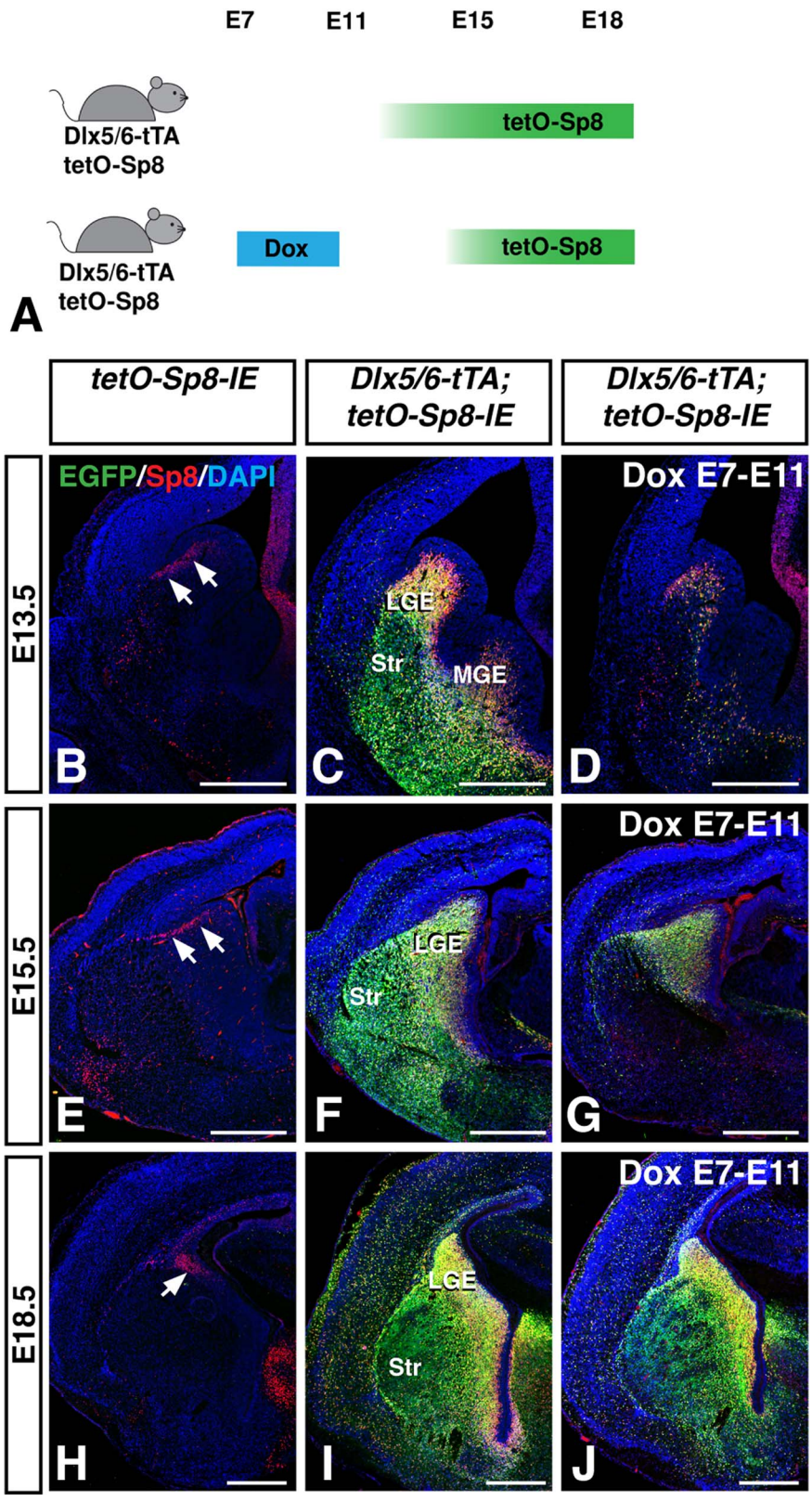

Figure 8. Doxycycline administration delays tTA-driven transgene expression. (*A*) Schematic illustrating our strategy to delay transgene activation. Administration of Dox in drinking water of females pregnant with *Dlx5/6-tTA;tetO-Sp8-IE* embryos from E7-E11 delayed transgene activation until around E14–15. (*B–D*) *Dlx5/6-tTA;tetO-Sp8-IE* mice (*C*) coexpress Sp8 and EGFP throughout the LGE and MGE compared to controls (*B*). E7–E11 Dox-treated *Dlx5/6-tTA;tetO-Sp8-IE* mice (*D*) show minimal transgene expression at E13.5. (*E–G*), By E15.5, Dox-treated *Dlx5/6-tTA;tetO-Sp8-IE* embryos (*G*) begin to misexpress Sp8 and EGFP throughout the SVZ, but considerably less than that in non-Dox-treated embryos (*F*). (*H–J*) By E18.5 embryos that were Dox-treated from E7-E11 (*J*) misexpress Sp8 and EGFP at similar levels to untreated embryos (*I*) in both the LGE and striatum. LGE, lateral ganglionic eminence; MGE, medial ganglionic eminence; Str, striatum. Scale bars: 500 µm.

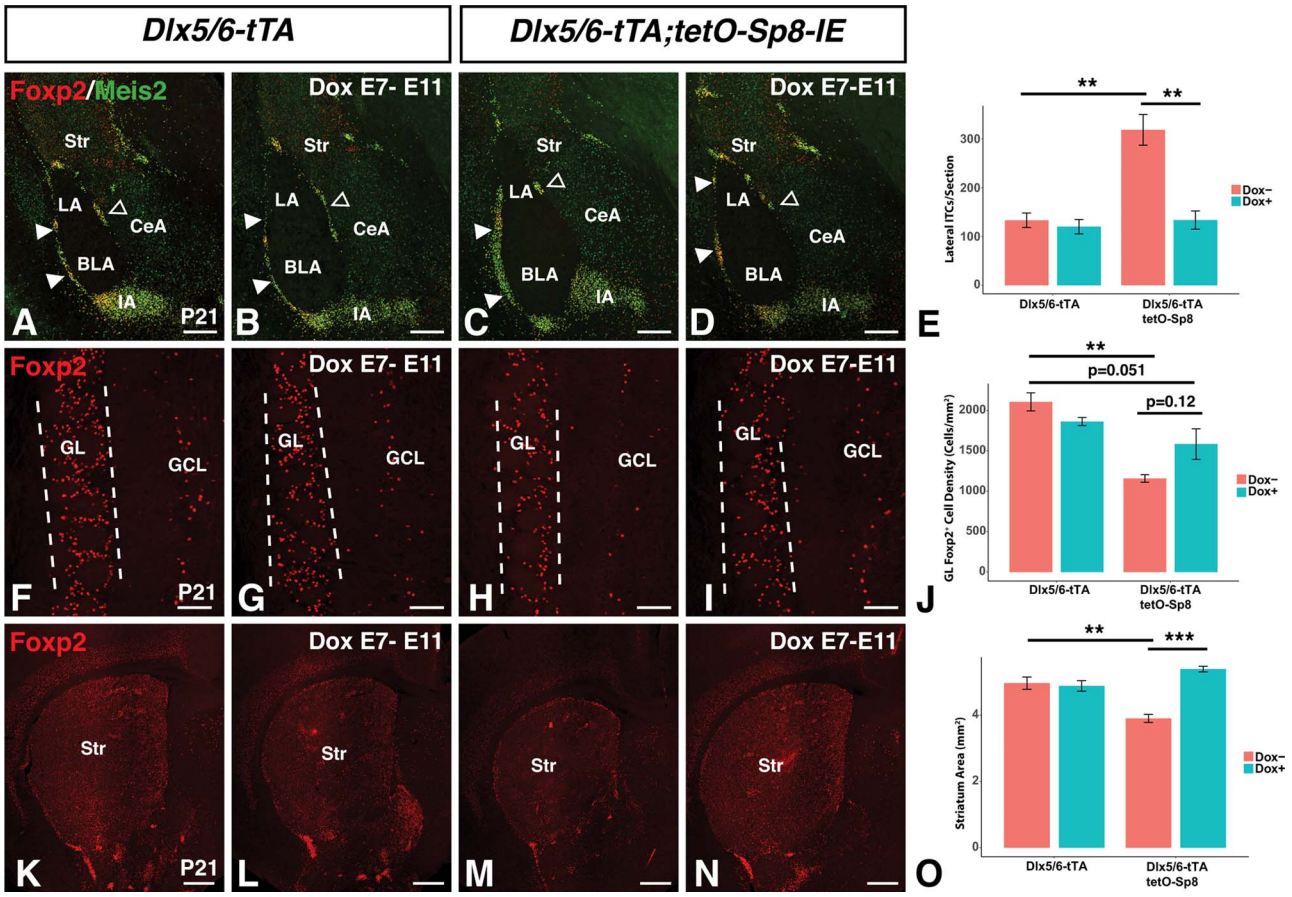

Figure 9. Dox delayed *Sp8* misexpression rescues ITC and striatum phenotypes. (*A–E*) Immunofluorescence (*A–D*) and quantification (*E*) illustrating the normalization of lateral ITC (solid arrowheads) numbers in *Sp8* misexpressing mice administered doxycycline from E7 to E11 (*D*) as compared to the untreated *Sp8* missexpressing mice (*C*). Note, Dox treatment of *Sp8* misexpressing mice (*D*) resulted in nearly identical numbers of ITCs as in the control mice (*A*,*B*). (*F-J*) Immunofluorescence (*F–I*) and quantification (*J*) showing a significant reduction in Foxp2$^+$ interneurons in the GL (between the dashed lines) of Sp8 missexpressing mice (*H*) as compared to controls (*F*). Furthermore, the reduction in Foxp2+ GL interneurons was not significantly improved after Dox treatment from E7 to E11 in *Sp8* misexpressing mice (*I*). (*K–O*) Immunofluorescence (*K–N*) and quantification (*O*) illustrating restoration of normal striatum size in *Sp8* misexpressing mice administered doxycycline from E7 to E11 (*N*) as compared to the significantly reduced striatum in the untreated *Sp8* misexpressing mice (*M*). Note that the striatum size in Dox-treated *Sp8* misexpressing mice appeared similar to that in the control mice (*K*,*L*). Data are represented as mean ± SEM and stats were performed using a two-way ANOVA with a post hoc Tukey HSD, $^{**}P < 0.01$, $^{***}P < 0.001$. BLA, basolateral amygdala; CeA, central amygdala; GCL, granule cell layer; GL glomerular layer; IA, main intercalated mass; LA, lateral amygdala; Str, striatum. Scale bars: *A–D*, 250 µm; *F–I*, 100 µm; *K–N*, 500 µm.

molecular heterogeneity in the LGE by identifying unique effects of the transcription factor Sp8 in 3 distinct LGE-derived neuronal populations: amygdala ITCs; OB interneurons; and SPNs. Our study supports previous reports showing Sp8 expression at embryonic timepoints in the dLGE and in the primary derivatives the of dLGE, namely ITCs and OB interneurons (Stenman et al. 2003a; Waclaw et al. 2006, 2010). At postnatal timepoints, Sp8 expression persists in the mouse SVZ, particularly in the dorsolateral portion which largely derives from progenitors in the LGE (Young et al. 2007). Furthermore, Sp8 remains expressed in SVZ derived neuroblasts of the RMS and interneurons of the OB. Previous studies have shown a distinct requirement for Sp8 in the CR$^+$ subpopulation of OB interneurons (Waclaw et al. 2006). Using a short-term fate-mapping approach (i.e., *Sp8-EGFP* BAC mice), we show that progeny of *Sp8*-expressing cells are detected among all the major populations of GL interneurons, but that CR$^+$ represents the most common fate among Sp8 derived interneurons. This finding is in agreement with observations that *Sp8/Sp9* double mutants exhibit loss of the TH$^+$ as well as CR$^+$ subtypes (Li et al. 2018), and that in the RMS, Sp8 is transiently expressed in neuroblasts from progenitor regions which produce all 3 interneuron lineages whereas maintained Sp8 expression occurs primarily in mature CR$^+$ interneurons (Waclaw et al. 2006; Gaborieau et al. 2018).

In this work, we have also generated and characterized the *Dlx5/6-tTA* transgenic mouse, which represents a novel tool to probe the molecular circuitry that shapes the developing ventral telencephalon. The *Dlx5/6* enhancer has previously been shown to drive reporter activity within the SVZ of the ventral telencephalon from E12.5 onward (Zerucha et al. 2000; Stenman et al. 2003b; Allen et al. 2007; Waclaw et al. 2010). In agreement with these reports, the *Dlx5/6-tTA* transgene is sufficient to drive transgene expression from a *tetO* promoter robustly throughout the SVZ at embryonic timepoints. With this transgenic tool, we built upon previous work demonstrating the utility of this double transgenic gain-of-function system for the temporal control of gene over/misexpression. Dox administration from E7-E11 was shown to be sufficient to suppress *tetO*-driven transgene expression until around E14–15.

Sp8 has previously been shown to be required for normal generation of amygdala ITCs (Waclaw et al. 2010). In the current work, we show that Sp8 is also sufficient to increase the numbers of ITCs generated from *Dlx5/6*-expressing progenitors. Moreover, this Sp8 driven ITC increase is dependent on the upregulation of the transcription factor *Tshz1* in the LGE. Conversely, combined deletion of Sp8 and Sp9 is sufficient to ablate *Tshz1* expression in the LGE (Li et al. 2018). We find that in addition to regulating the total number of ITCs, *Tshz1* gene dosage also affects the medial-lateral distribution of ITCs with fewer laterally located ITCs observed in *Tshz1* heterozygotes. Similarly, in *Tshz1* null animals, all ITCs are clustered medially (Kuerbitz et al. 2018). Factors functioning downstream of *Tshz1* to regulate ITC migration have not been established, but one interesting candidate is *Prokr2*. ITC *Prokr2* expression is downregulated in *Tshz1* knockout mice (Kuerbitz et al. 2018), and the OB interneurons of *Tshz1* and *Sp8/Sp9* mutants show loss of *Prokr2* as well as perturbed interneuron migration (Ragancokova et al. 2014; Li et al. 2018). *Prokr2* mutant mice show similar defects in OB interneuron migration (Matsumoto et al. 2006; Prosser et al. 2007). Indeed, a recent study has shown that Prok2/Prokr2 signaling is required for the normal tangential and radial migration of most (i.e., approximately 75%) of GABAergic OB interneurons (Wen et al. 2019). Although further work is necessary, these observations establish the possibility that *Sp8*, *Tshz1*, and *Prokr2* act in a pathway to regulate the migration of multiple neuronal subtypes (i.e., ITCs and OB interneurons).

Like ITCs, the CR^+ interneurons of the GL have been shown to depend on Sp8 for their normal development (Waclaw et al. 2006). Interestingly, although the present work suggests that ectopic Sp8 within LGE progenitors is sufficient to upregulate *Tshz1* gene expression in a significant portion of the LGE cells, *Tshz1* expression has never been reported in CR^+ OB interneurons. Moreover, while loss of *Tshz1* severely impairs CB^+ interneuron generation, CR^+ neurogenesis is maintained in *Tshz1* mutants (Ragancokova et al. 2014). These distinct *Tshz1* expression patterns and dependencies in dLGE-derived *Sp8* lineages suggest the existence of 2 divergent molecular pathways downstream of Sp8 in the ventral telencephalon: a *Tshz1* dependent pathway that gives rise to ITCs and a *Tshz1* independent lineage that contributes to CR^+ interneuron development.

Both ITCs and GL CB^+ interneurons are characterized by expression of Foxp2 and Meis2 and depend on *Tshz1* for their proper generation and/or migration (Kaoru et al. 2010; Ragancokova et al. 2014; Fujiwara and Cave 2016; Kuerbitz et al. 2018). The factors governing the fate of the dLGE progenitors that give rise to these molecularly similar populations remain poorly understood. Interestingly, although forced *Sp8* expression is sufficient to increase *Tshz1* expression in progenitors throughout much of the LGE SVZ, it did not increase the numbers of $CB^+/Foxp2^+$ OB GL interneurons. In fact, a dramatic loss of $CB^+/Foxp2^+$ OB interneurons was observed in *Sp8* misexpressing animals. This was in stark contrast to the increased number of $Foxp2^+$ ITCs observed in the *Sp8* misexpressing amygdala. As shown in the short-term fate maps (i.e., *Sp8-EGFP* BAC transgene), the $Sp8^+$ neuroblasts do not appear to give rise to large numbers of $CB^+/Foxp2^+$ GL interneurons and thus, it may be the case that these 2 cell types derive from separate dLGE lineages whose migration and/or proliferation capacities are oppositely affected by Sp8. Our findings suggest that *Sp8* and *Tshz1* may interact genetically in the development of these 2 dLGE neuronal subtypes. In fact, reducing the *Tshz1* dosage in *Sp8* misexpressing animals, normalized $Foxp2^+$ ITC numbers and improved OB $Foxp2^+$ (i.e., CB^+) GL numbers. Thus, high levels of *Tshz1* expression together with *Sp8* appears to promote $Foxp2^+$ ITCs from dLGE progenitors, whereas lower levels of *Tshz1* together with *Sp8* allows for a more normal development of $Foxp2^+$ (i.e., CB^+) GL interneurons from these progenitors. It could be speculated that the high levels of Tshz1 together with Sp8 may respecify some dLGE progenitors from $Foxp2^+/CB^+$ GL interneurons toward $Foxp2^+$ ITCs.

Other potential sources of the increased numbers of ITCs observed in *Sp8* misrexpressing mice include an expanded progenitor pool or a respecification of vLGE progenitors. Misexpression of Sp8 in the adult SVZ causes reductions in the number of neural stem cells and accelerated cell cycle exit (Gaborieau et al. 2018), suggesting that Sp8 overexpression is unlikely to expand the pool of ITC progenitors. Moreover, restricted misexpression of Sp8 in $Isl1^+$ vLGE progenitors was not sufficient to divert vLGE cells to ITC clusters from the striatum, suggesting that the vLGE is unlikely to be the source of additional ITCs in Sp8 misexpressing mice. However, *Dlx5/6* genes are expressed in earlier progenitors than *Isl1* (Stenman et al. 2003a; Ehrman et al. 2013), and therefore it is possible that there exists a window prior to *Isl1* expression in which the *Dlx5/6* lineage vLGE neurons are susceptible to respecification by Sp8.

The OBs of Sp8 misexpressing mice contained significantly fewer $Meis2^+$ interneurons in the GL at both embryonic and postnatal timepoints indicating a reduction of the total GL interneuron population. This was not the case for $Meis2^+$ GCL interneurons. In addition to diversion of precursors to alternative fates (ITCs), other possible mechanisms underlying the reduction in GL interneurons include decreased neurogenesis, decreased survival, and impaired migration. Consistent with disrupted migration of neuroblasts to the OB, we observed a disorganized SVZ containing dense clusters of ectopic cells including a number CR^+ neurons in Sp8 misexpressing mice, which may represent neuroblasts that failed to migrate appropriately and subsequently differentiated prematurely. Interestingly, loss of Sp8 also results in abnormal expression of CR^+ and CB^+ neurons in the RMS (Waclaw et al. 2006). Therefore, Sp8 LOF or GOF disrupts normal RMS migration and differentiation suggesting a fine balance of Sp8 levels for OB interneuron development.

Gaborieau et al. (2018) overexpressed Sp8 via electroporation of the postnatal ventricular wall and observed normal anterior–posterior distribution of electroporated cells in the RMS suggesting that Sp8 does not influence the migratory capacity of postnatal neuroblasts. However, their approach produced fairly limited Sp8 overexpression. Our transgenic model results in early and broad misexpression of Sp8. Neuroblasts in the RMS normally migrate via chain migration through "astroglial tubes" (Lois et al. 1996; Wichterle et al. 1999). The embryonic Sp8 misexpression model may disrupt the normal formation of the RMS infrastructure which results in the broad OB interneuron defects observed. Indeed, it has been previously reported that the presence of *Dab1* deficient Purkinje cells in the hippocampus of chimeric mice is sufficient to disrupt the migration of wild-type cells, providing evidence for a noncell-autonomous "community effect" (Yang et al. 2002). Further experiments involving mosaic misexpression of Sp8 at embryonic stages will be necessary to test if similar effects occur in the RMS.

Our results demonstrate that *Sp8* misexpression affects distinct neuronal subpopulations at different timepoints. Early

misexpression of *Sp8* was sufficient to increase amygdala ITC numbers from LGE (presumably dLGE) progenitors whereas late *Sp8* expression (i.e., after E15) was incapable of increasing ITC numbers. This is in line with the fact that ITC neurogenesis is completed by late embryonic time points (Bayer 1980). Similarly, delaying Sp8 misexpression also rescues Sp8-induced reduction of striatal size since a large amount of striatal neurogenesis occurs during our experimental Dox treatments when the transgene is repressed (Bayer 1984; Kelly et al. 2018). Conversely, delayed misexpression of *Sp8* in LGE progenitors still results in a reduction of CB^+ OB interneurons, which fits with the fact that these neurons are generated throughout the embryonic and early postnatal period (Batista-Brito et al. 2014).

The present work underscores the heterogeneity that exists within LGE progenitors and suggests that Sp8 plays an important role in regulating the proportion of different neuronal subtypes produced from the LGE progenitor domains. However, the effect of Sp8 overexpression varied significantly between cell-types. For example, although Sp8 increased *Tshz1* expression in most LGE SVZ cells leading to increased ITCs, OB interneuron development was disrupted with altered migration in CR^+ interneurons and reduced numbers of TH^+ and CB^+ interneurons. The molecular mediators of these distinct Sp8- and Tshz1-dependent effects are interesting to speculate about and may include differences in the transcription factor milieu resulting in different Sp8 binding partners between populations or differences in chromatin structure leading to differences in Sp8 target accessibility. In one example of context specific effects of transcription factors, recent work has shown that the LGE transcription factor Gsx2 upregulates the expression of the neurogenic factor Ascl1 but delays neurogenesis by physically interacting with Ascl1 and limiting its ability to bind to its neurogenic target genes (Roychoudhury et al. 2020). Similarly, Pax6 has been shown to interact with the TALE homeodomain transcription factor Meis2, and this interaction is essential for Pax6's prodopaminergic function (Agoston et al. 2014).

In summary, we have generated a new transgenic mouse (*Dlx5/6-tTA*) to develop an *Sp8* misexpression system used to examine known and novel an spects of heterogeneity in LGE progenitors. At early time points, a population of LGE (presumably dLGE) progenitors respond to *Sp8* misexpression by upregulating *Tshz1* and subsequently giving rise to ITCs. Conversely, ectopic *Sp8* expression results in reduced OB interneuron subtypes (e.g., TH and CB) possibly as a result of respecification toward ITC fates. Finally, Sp8 misexpression in vLGE progenitors leads to severe reductions in SPNs but no apparent respecification into dLGE fates.

Supplementary Material

Supplementary Material can be found at *Cerebral Cortex* online.

Notes

We thank Marc Ekker for providing the *Dlx5/6* enhancer construct and Alistair Garratt for providing the $Tshz1^{flox}$ mice. *Conflict of Interest:* None declared.

Funding

National Institutes of Health grants R01 NS044080 to K.C. and R01 MH090740 to R.R.W. and K.C.

References

Agoston Z, Heine P, Brill MS, Grebbin BM, Hau A-C, Kallenborn-Gerhardt W, Schramm J, Götz M, Schulte D. 2014. Meis2 is a Pax6 co-factor in neurogenesis and dopaminergic periglomerular fate specification in the adult olfactory bulb. *Development*. 141:28–38.

Allen ZJ, Waclaw RR, Colbert MC, Campbell K. 2007. Molecular identity of olfactory bulb interneurons: transcriptional codes of periglomerular neuron subtypes. *J Mol Histol*. 38:517–525.

Anderson KD, Reiner A. 1991. Immunohistochemical localization of DARPP-32 in striatal projection neurons and striatal interneurons: implications for the localization of D1-like dopamine receptors on different types of striatal neurons. *Brain Res*. 568:235–243.

Batista-Brito R, Close J, Machold R, Fishell G. 2014. The distinct temporal origins of olfactory bulb interneuron subtypes. *J Neurosci*. 28:3966–3975.

Bayer SA. 1980. Quantitative 3H-thymidine radiographic analyses of neurogenesis in the rat amygdala. *J Comp Neurol*. 194:845–875.

Bayer SA. 1984. Neurogenesis in the rat neostriatum. *Int J Dev Neurosci*. 2:163–175.

Bayer SA, Altman J, Russo RJ, Dai X, Simmons JA. 1991. Cell migration in the rat embryonic neocortex. *J Comp Neurol*. 307:499–516.

Borello U, Madhavan M, Vilinsky I, Faedo A, Pierani A, Rubenstein J, Campbell K. 2014. Sp8 and COUP-TF1 reciprocally regulate patterning and Fgf signaling in cortical progenitors. *Cereb Cortex*. 24:1409–1421.

Brill MS, Snapyan M, Wohlfrom H, Ninkovic J, Jawerka M, Mastick GS, Ashery-Padan R, Saghatelyan A, Berninger B, Götz M. 2008. A Dlx2- and Pax6-dependent transcriptional code for periglomerular neuron specification in the adult olfactory bulb. *J Neurosci*. 28:6439–6452.

Carney RSE, Alfonso TB, Cohen D, Dai H, Nery S, Stoica B, Slotkin J, Bregman BS, Fishell G, Corbin JG. 2006. Cell migration along the lateral cortical stream to the developing basal telencephalic limbic system. *J Neurosci*. 26:11562–11574.

Caubit X, Tiveron M-C, Cremer H, Fasano L. 2005. Expression patterns of the three Teashirt-related genes define specific boundaries in the developing and postnatal mouse forebrain. *J Comp Neurol*. 486:76–88.

Chang C-W, Tsai C-W, Wang H-F, Tsai H-C, Chen H-Y, Tsai T-F, Takahashi H, Li H-Y, Fann M-J, Yang C-W et al. 2004. Identification of a developmentally regulated striatum-enriched zinc-finger gene, Nolz-1, in the mammalian brain. *Proc Natl Acad Sci USA*. 101:2613–2618.

Chapman H, Waclaw RR, Pei Z, Nakafuku M, Campbell K. 2013. The homeobox gene Gsx2 controls the timing of oligodendroglial fate specification in mouse lateral ganglionic eminence progenitors. *Development*. 140:2289–2298.

Chen R, Lin C, You Y, Liu F. 2012. Characterization of immature and mature 5-hydroxytryptamine 3A receptor-expressing cells within the adult SVZ-RMS-OB system. *Neuroscience*. 227:180–190.

Cocas LA, Georgala PA, Mangin J-M, Clegg JM, Kessaris N, Haydar TF, Gallo V, Price DJ, Corbin JG. 2011. Pax6 is required at the telencephalic pallial–subpallial boundary for the generation of neuronal diversity in the postnatal limbic system. *J Neurosci*. 31:5313–5324.

Cocas LA, Miyoshi G, Carney RSE, Sousa VH, Hirata T, Jones KR, Fishell G, Huntsman MM, Corbin JG. 2009. Emx1-lineage

progenitors differentially contribute to neural diversity in the striatum and amygdala. *J Neurosci*. 29:15933–15946.

Dellovade TL, Pfaff DW, Schwanzel-Fukuda M. 1998. Olfactory bulb development is altered in small-eye (Sey) mice. *J Comp Neurol*. 402:402–418.

Duval ER, Javanbakht A, Liberzon I. 2015. Neural circuits in anxiety and stress disorders: a focused review. *Ther Clin Risk Manag*. 11:115–126.

Ehrman LA, Mu X, Waclaw RR, Yoshida Y, Vorhees CV, Klein WH, Campbell K. 2013. The LIM homeobox gene Isl1 is required for the correct development of the striatonigral pathway in the mouse. *Proc Natl Acad Sci USA*. 110:E4026–E4035.

Fremeau RT, Duncan GE, Fornaretto MG, Dearry A, Gingrich JA, Breese GR, Caron MG. 1991. Localization of D1 dopamine receptor mRNA in brain supports a role in cognitive, affective, and neuroendocrine aspects of dopaminergic neurotransmission. *Proc Natl Acad Sci USA*. 88:3772–3776.

Fujiwara N, Cave JW. 2016. Partial conservation between mice and humans in olfactory bulb interneuron transcription factor codes. *Front Neurosci*. 10:337.

Gaborieau E, Hurtado-Chong A, Fernández M, Azim K, Raineteau O. 2018. A dual role for the transcription factor Sp8 in postnatal neurogenesis. *Sci Rep*. 8:1–10.

Gerfen CR, Engber TM, Mahan LC, Susel Z, Chase TN, Monsma FJ, Sibley DR. 1990. D1 and D2 dopamine receptor-regulated gene expression of striatonigral and striatopallidal neurons. *Science*. 250:1429–1432.

Gong S, Zheng C, Doughty ML, Losos K, Didkovsky N, Schambra UB, Nowak NJ, Joyner A, Leblanc G, Hatten ME et al. 2003. A gene expression atlas of the central nervous system based on bacterial artificial chromosomes. *Nature*. 425:917–925.

Gossen M, Bujard H. 1992. Tight control of gene expression in mammalian cells by tetracycline-responsive promoters. *Proc Natl Acad Sci USA*. 89:5547–5551.

Haba H, Nomura T, Suto F, Osumi N. 2009. Subtype-specific reduction of olfactory bulb interneurons in Pax6 heterozygous mutant mice. *Neurosci Res*. 65:116–121.

Hack MA, Saghatelyan A, de Chevigny A, Pfeifer A, Ashery-Padan R, Lledo P-M, Götz M. 2005. Neuronal fate determinants of adult olfactory bulb neurogenesis. *Nat Neurosci*. 8:865–872.

Hinds JW. 1968. Autoradiographic study of histogenesis in the mouse olfactory bulb. I. Time of origin of neurons and neuroglia. *J Comp Neurol*. 134:287–304.

Hirata T, Li P, Lanuza GM, Cocas LA, Huntsman MM, Corbin JG. 2009. Identification of distinct telencephalic progenitor pools for neuronal diversity in the amygdala. *Nat Neurosci*. 12:141–149.

Hsieh-Li HM, Witte DP, Szucsik JC, Weinstein M, Li H, Potter SS. 1995. Gsh-2, a murine homeobox gene expressed in the developing brain. *Mech Dev*. 50:177–186.

Jacobsen KX, Höistad M, Staines WA, Fuxe K. 2006. The distribution of dopamine D1 receptor and μ-opioid receptor 1 receptor immunoreactivities in the amygdala and interstitial nucleus of the posterior limb of the anterior commissure: relationships to tyrosine hydroxylase and opioid peptide terminal systems. *Neuroscience*. 141:2007–2018.

Kaoru T, Liu F-C, Ishida M, Oishi T, Hayashi M, Kitagawa M, Shimoda K, Takahashi H. 2010. Molecular characterization of the intercalated cell masses of the amygdala: implications for the relationship with the striatum. *Neuroscience*. 166:220–230.

Kelly SM, Raudales R, He M, Lee JH, Kim Y, Gibb LG, Wu P, Matho K, Osten P, Graybiel AM et al. 2018. Radial glial lineage progression and differential intermediate progenitor amplification underlie striatal compartments and circuit organization. *Neuron* 99. e4:345–361.

Kistner A, Gossen M, Zimmermann F, Jerecic J, Ullmer C, Lübbert H, Bujard H. 1996. Doxycycline-mediated quantitative and tissue-specific control of gene expression in transgenic mice. *Proc Natl Acad Sci USA*. 93:10933–10938.

Kohwi M, Osumi N, Rubenstein JLR, Alvarez-Buylla A. 2005. Pax6 is required for making specific subpopulations of granule and periglomerular neurons in the olfactory bulb. *J Neurosci*. 25:6997–7003.

Kosaka K, Toida K, Aika Y, Kosaka T. 1998. How simple is the organization of the olfactory glomerulus?: the heterogeneity of so-called periglomerular cells. *Neurosci Res*. 30:101–110.

Kosaka T, Hataguchi Y, Hama K, Nagatsu I, Wu JY. 1985. Coexistence of immunoreactivities for glutamate decarboxylase and tyrosine hydroxylase in some neurons in the periglomerular region of the rat main olfactory bulb: possible coexistence of gamma-aminobutyric acid (GABA) and dopamine. *Brain Res*. 343:166–171.

Kosaka T, Kosaka K. 2012. Further characterization of the juxtaglomerular neurons in the mouse main olfactory bulb by transcription factors, Sp8 and Tbx21. *Neurosci Res*. 73:24–31.

Kuerbitz J, Arnett M, Ehrman S, Williams MT, Vorhees CV, Fisher SE, Garratt AN, Muglia LJ, Waclaw RR, Campbell K. 2018. Loss of intercalated cells (ITCs) in the mouse amygdala of Tshz1 mutants correlates with fear, depression, and social interaction phenotypes. *J Neurosci*. 38:1160–1177.

Laugwitz K-L, Moretti A, Lam J, Gruber P, Chen Y, Woodard S, Lin L-Z, Cai C-L, Lu MM, Reth M et al. 2005. Postnatal isl1+ cardioblasts enter fully differentiated cardiomyocyte lineages. *Nature*. 433:647–653.

Li J, Wang C, Zhang Z, Wen Y, An L, Liang Q, Xu Z, Wei S, Li W, Guo T et al. 2018. Transcription factors Sp8 and Sp9 coordinately regulate olfactory bulb interneuron development. *Cereb Cortex*. 28:3278–3294.

Li X, Sun C, Lin C, Ma T, Madhavan MC, Campbell K, Yang Z. 2011. The transcription factor Sp8 is required for the production of parvalbumin-expressing interneurons in the olfactory bulb. *J Neurosci*. 31:8450–8455.

Liu JK, Ghattas I, Liu S, Chen S, Rubenstein JL. 1997. Dlx genes encode DNA-binding proteins that are expressed in an overlapping and sequential pattern during basal ganglia differentiation. *Dev Dyn*. 210:498–512.

Lledo P-M, Merkle FT, Alvarez-Buylla A. 2008. Origin and function of olfactory bulb interneuron diversity. *Trends Neurosci*. 31:392–400.

Lois C, Alvarez-Buylla A. 1994. Long-distance neuronal migration in the adult mammalian brain. *Science*. 264:1145–1148.

Lois C, García-Verdugo JM, Alvarez-Buylla A. 1996. Chain migration of neuronal precursors. *Science*. 271:978–981.

López-Juárez A, Howard J, Ullom K, Howard L, Grande A, Pardo A, Waclaw R, Sun Y-Y, Yang D, Kuan C-Y et al. 2013. Gsx2 controls region-specific activation of neural stem cells and injury-induced neurogenesis in the adult subventricular zone. *Genes Dev*. 27:1272–1287.

Luskin MB. 1993. Restricted proliferation and migration of postnatally generated neurons derived from the forebrain subventricular zone. *Neuron*. 11:173–189.

Madisen L, Zwingman TA, Sunkin SM, Oh SW, Zariwala HA, Gu H, Ng LL, Palmiter RD, Hawrylycz MJ, Jones AR et al. 2010. A robust and high-throughput Cre reporting and

characterization system for the whole mouse brain. *Nat Neurosci*. 13:133–140.

Maletic V, Robinson M, Oakes T, Iyengar S, Ball SG, Russell J. 2007. Neurobiology of depression: an integrated view of key findings. *Int J Clin Pract*. 61:2030–2040.

Matsumoto S, Yamazaki C, Masumoto K, Nagano M, Naito M, Soga T, Hiyama H, Matsumoto M, Takasaki J, Kamohara M et al. 2006. Abnormal development of the olfactory bulb and reproductive system in mice lacking prokineticin receptor PKR2. *Proc Natl Acad Sci USA*. 103:4140–4145.

Mayer C, Hafemeister C, Bandler RC, Machold R, Brito RB, Jaglin X, Allaway K, Butler A, Fishell G, Satija R. 2018. Developmental diversification of cortical inhibitory interneurons. *Nature*. 555:457–462.

Merchan-Sala P, Nardini D, Waclaw RR, Campbell K. 2017. Selective neuronal expression of the SoxE factor, Sox8, in direct pathway striatal projection neurons of the developing mouse brain. *J Comp Neurol*. 525:2805–2819.

Nagayama S, Homma R, Imamura F. 2014. Neuronal organization of olfactory bulb circuits. *Front Neural Circuits*. 8:98.

Olsson M, Campbell K, Turnbull D. 1997. Specification of mouse telencephalic and mid-hindbrain progenitors following heterotopic ultrasound-guided embryonic transplantation. *Neuron*. 19:761–772.

Parrish-Aungst S, Shipley MT, Erdelyi F, Szabo G, Puche AC. 2007. Quantitative analysis of neuronal diversity in the mouse olfactory bulb. *J Comp Neurol*. 501:825–836.

Pei Z, Wang B, Chen G, Nagao M, Nakafuku M, Campbell K. 2011. Homeobox genes Gsx1 and Gsx2 differentially regulate telencephalic progenitor maturation. *Proc Natl Acad Sci U S A*. 108:1675–1680.

Porteus MH, Bulfone A, Ciaranello RD, Rubenstein JLR. 1991. Isolation and characterization of a novel cDNA clone encoding a homeodomain that is developmentally regulated in the ventral forebrain. *Neuron*. 7:221–229.

Precious SV, Kelly CM, Reddington AE, Vinh NN, Stickland RC, Pekarik V, Scherf C, Jeyasingham R, Glasbey J, Holeiter M et al. 2016. FoxP1 marks medium spiny neurons from precursors to maturity and is required for their differentiation. *Exp Neurol*. 282:9–18.

Price M, Lemaistre M, Pischetola M, Lauro RD, Duboule D. 1991. A mouse gene related to distal-less shows a restricted expression in the developing forebrain. *Nature*. 351:748–751.

Prosser HM, Bradley A, Caldwell MA. 2007. Olfactory bulb hypoplasia in Prokr2 null mice stems from defective neuronal progenitor migration and differentiation. *Eur J Neurosci*. 26:3339–3344.

Qin S, Madhavan M, Waclaw RR, Nakafuku M, Campbell K. 2016. Characterization of a new Gsx2-cre line in the developing mouse telencephalon. *Genesis*. 54:542–549.

Ragancokova D, Rocca E, Oonk AMM, Schulz H, Rohde E, Bednarsch J, Feenstra I, Pennings RJE, Wende H, Garratt AN. 2014. TSHZ1-dependent gene regulation is essential for olfactory bulb development and olfaction. *J Clin Invest*. 124:1214–1227.

Robinson GW, Wray S, Mahon KA. 1991. Spatially restricted expression of a member of a new family of murine distal-less homeobox genes in the developing forebrain. *New Biol*. 3:1183–1194.

Roychoudhury K, Salomone J, Qin S, Cain B, Adam M, Potter SS, Nakafuku M, Gebelein B, Campbell K. 2020. Physical interactions between Gsx2 and Ascl1 balance progenitor expansion versus neurogenesis in the mouse lateral ganglionic eminence. *Development*. 147:dev185348.

Sahara S, Kawakami Y, Belmonte JCI, O'Leary DD. 2007. Sp8 exhibits reciprocal induction with Fgf8 but has an opposing effect on anterior-posterior cortical area patterning. *Neural Dev*. 2:10.

Simeone A, Acampora D, Pannese M, D'Esposito M, Stornaiuolo A, Gulisano M, Mallamaci A, Kastury K, Druck T, Huebner K. 1994. Cloning and characterization of two members of the vertebrate dlx gene family. *Proc Natl Acad Sci USA*. 91:2250–2254.

Stenman J, Toresson H, Campbell K. 2003a. Identification of two distinct progenitor populations in the lateral ganglionic eminence: implications for striatal and olfactory bulb neurogenesis. *J Neurosci*. 23:167–174.

Stenman J, Yu RT, Evans RM, Campbell K. 2003b. Tlx and Pax6 cooperate genetically to establish the pallio-subpallial boundary in the embryonic mouse telencephalon. *Development*. 130:1113–1122.

Takahashi K, Liu FC, Hirokawa K, Takahashi H. 2008. Expression of Foxp4 in the developing and adult rat forebrain. *J Neurosci Res*. 86:3106–3116.

Tamura S, Morikawa Y, Iwanishi H, Hisaoka T, Senba E. 2004. Foxp1 gene expression in projection neurons of the mouse striatum. *Neuroscience*. 124:261–267.

Toresson H, Mata de Urquiza A, Fagerstrom C, Perlmann T, Campbell K. 1999. Retinoids are produced by glia in the lateral ganglionic eminence and regulate striatal neuron differentiation. *Development*. 126:1317.

Toresson H, Potter SS, Campbell K. 2000. Genetic control of dorsal-ventral identity in the telencephalon: opposing roles for Pax6 and Gsh2. *Development*. 127:4361–4371.

Tucker ES, Polleux F, LaMantia AS. 2006. Position and time specify the migration of a pioneering population of olfactory bulb interneurons. *Dev Biol*. 297:387–401.

Waclaw RR, Allen ZJ II, Bell SM, Erdélyi F, Szabó G, Potter SS, Campbell K. 2006. The zinc finger transcription factor Sp8 regulates the generation and diversity of olfactory bulb interneurons. *Neuron*. 49:503–516.

Waclaw RR, Ehrman LA, Pierani A, Campbell K. 2010. Developmental origin of the neuronal subtypes that comprise the amygdalar fear circuit in the mouse. *J Neurosci*. 30: 6944–6953.

Waclaw RR, Wang B, Pei Z, Ehrman LA, Campbell K. 2009. Distinct temporal requirements for the homeobox gene Gsx2 in specifying striatal and olfactory bulb neuronal fates. *Neuron*. 63:451–465.

Walker FO. 2007. Huntington's disease. *The Lancet*. 369:218–228.

Wang C, You Y, Qi D, Zhou X, Wang L, Wei S, Zhang Z, Huang W, Liu Z, Liu F et al. 2014. Human and monkey striatal interneurons are derived from the medial ganglionic eminence but not from the adult subventricular zone. *J Neurosci*. 34:10906–10923.

Wang L, Sharma K, Deng H-X, Siddique T, Grisotti G, Liu E, Roos RP. 2008. Restricted expression of mutant SOD1 in spinal motor neurons and interneurons induces motor neuron pathology. *Neurobiol Dis*. 29:400–408.

Yun K, Potter S, Rubenstein JL. 2001. Gsh2 and Pax6 play complementary roles in dorsoventral patterning of the mammalian telencephalon. *Development*. 128:193–205.

Wei B, Nie Y, Li X, Wang C, Ma T, Huang Z, Tian M, Sun C, Cai Y, You Y et al. 2011. Emx1-expressing neural stem cells in the subventricular zone give rise to new interneurons in the ischemic injured striatum. *Eur J Neurosci*. 33: 819–830.

Wen Y, Zhang Z, Li Z, Liu G, Tao G, Song X, Xu Z, Shang Z, Guo T, Su Z et al. 2019. The PROK2/PROKR2 signaling pathway is required for the migration of most olfactory bulb interneurons. *J Comp Neurol*. 527:2931–2947.

Wichterle H, Garcia-Verdugo JM, Herrera DG, Alvarez-Buylla A. 1999. Young neurons from medial ganglionic eminence disperse in adult and embryonic brain. *Nat Neurosci*. 2:461–466.

Yang H, Jensen P, Goldowitz D. 2002. The community effect and Purkinje cell migration in the cerebellar cortex: analysis of scrambler chimeric mice. *J Neurosci*. 22:464–470.

Young KM, Fogarty M, Kessaris N, Richardson WD. 2007. Subventricular zone stem cells are heterogeneous with respect to their embryonic origins and neurogenic fates in the adult olfactory bulb. *J Neurosci*. 27:8286–8296.

Zerucha T, Stühmer T, Hatch G, Park BK, Long Q, Yu G, Gambarotta A, Schultz JR, Rubenstein JLR, Ekker M. 2000. A highly conserved enhancer in the Dlx5/Dlx6Intergenic region is the site of cross-regulatory interactions betweenDlx genes in the embryonic forebrain. *J Neurosci*. 20: 709–721.